Singlet and Triplet Excited States of Emissive, Conjugated Bis(porphyrin) Compounds Probed by Optical and EPR Spectroscopic Methods

Renée Shediac,[†] Mike H. B. Gray,[†] H. Tetsuo Uyeda,[†] Robert C. Johnson,[§] Joseph T. Hupp,[§] Paul J. Angiolillo,*[,‡] and Michael J. Therien*[,†]

Contribution from the Department of Chemistry, University of Pennsylvania, Philadelphia, Pennsylvania 19104-6323, the Department of Chemistry, Northwestern University, Evanston, Illinois 60208, and the Department of Physics, Mathematics and Computer Science, University of the Sciences in Philadelphia, 600 South 43rd Street, Philadelphia, Pennsylvania 19104-4495

Received November 9, 1999. Revised Manuscript Received May 3, 2000

Abstract: The nature of the singlet and triplet excited states of a series of *meso*-to-*meso* ethyne-linked bis(porphyrin) compounds was probed by electronic absorption, polarized pump−probe fluorescence, electron paramagnetic resonance (EPR), electroabsorption (Stark), and transient triplet−triplet absorption spectroscopic methods. Pump−probe fluorescence anisotropy experiments show that the presence of *meso*-ethynyl substituents drives a reorientation of orthogonal *x*- and *y*-polarized singlet excited states in the macrocycle frame of reference with respect to that evinced for conventional free-base porphyrin chromophores. Analogous experiments in conjugated bis(porphyrin) species bis[(5,5′,-10,20-bis[3″,5″-(di-*tert* -butyl)phenyl]porphinato)zinc(II)]ethyne, 5-[10,20-bis[3″,5″-(di-*tert*-butyl)phenyl]porphinato)zinc(II)]-5′-[10′,20′-bis[3″,5″-(di-*tert*-butyl)phenyl]porphyryl]-ethyne, and bis[5,5′,-10,20-bis[3″,5″-(di-*tert*-butyl)phenyl]porphyryl]ethyne demonstrate substantial energetic splittings of the *x*- and *y*-polarized S_1 states. The magnitude of this energetic gap results in the complete suppression of population exchange between excited states having orthogonal polarizations on the time scale of these measurements, and gives rise to singly degenerate emitting states polarized exclusively along the axis defined by the ethyne moiety. Stark spectroscopic experiments show that the electronically symmetric *meso*-to-*meso* ethyne-bridged bis[(porphinato)zinc(II)] complex exhibits changes in dipole moment with respect to the ground state in its respective *x*-polarized S_2 and S_1 states. The EPR spectra of the low-lying photoexcited triplet excited states of these conjugated bis(porphyrin) compounds and their ethyne-substituted porphyrinic building blocks show an evolution in the $|D|$ and $|E|$ ZFS parameters with augmented conjugation consistent with a progressing oblate-to-prolate spin transition that causes the direction of largest dipolar interaction to align along the vector defined by the conjugated ethyne moiety. Conjugated arrays based on *meso*-ethyne elaborated porphyrin and (porphinato)zinc(II) precursors thus constitute an unusual class of oligomeric porphyrin species in that once a threshold level of conjugation is reached, the optical and magnetic principal axis systems become coincident.

Introduction

Understanding energy and electron migration reactions in multichromophoric assemblies is essential for biomimetic modeling of energy transduction, and the eventual design and development of supramolecular systems based on biological pigments relevant to artificial photosynthesis,[1−15] materials chemistry,[16−19] and optoelectronics.[20−28] Designing molecular-based structures for such applications will likely require the ability to modulate the nature and magnitude of electronic interactions between pigments in a facile manner. Toward this goal, we have synthesized a compact set of conjugated oligo-

[†] University of Pennsylvania.
[§] Northwestern University.
[‡] University of the Sciences in Philadelphia.

(1) Lin, V. S.-Y.; DiMagno, S. G.; Therien, M. J. *Science* **1994**, *264*, 1105−1111.
(2) Lin, V. S.-Y.; Therien, M. J. *Chem. Eur. J.* **1995**, *1*, 645−651.
(3) Hsiao, J.-S.; Krueger, B. P.; Wagner, R. W.; Johnson, T. E.; Delaney, J. K.; Mauzerall, D. C.; Fleming, G. R.; Lindsey, J. S.; Bocian, D. F.; Donohoe, R. J. *J. Am. Chem. Soc.* **1996**, *118*, 11181−11193.
(4) Van Patten, P. G.; Shreve, A. P.; Lindsey, J. S.; Donohue, R. J. *J. Phys. Chem. B* **1998**, *102*, 4209−4216.
(5) Osuka, A.; Nagata, T.; Maruyama, K.; Mataga, N.; Asahi, T.; Yamazaki, I.; Nishimura, Y. *Chem. Phys. Lett.* **1991**, *185*, 88−94.
(6) Osuka, A.; Nakajima, S.; Maruyama, K.; Mataga, N.; Asahi, T.; Yamazaki, I.; Nishimura, Y.; Ohno, T.; Nozaki, K. *J. Am. Chem. Soc.* **1993**, *115*, 4577−4589.
(7) Osuka, A.; Marumo, S.; Taniguchi, S.; Okada, T.; Mataga, N. *Chem. Phys. Lett.* **1994**, *230*, 144−148.
(8) Sessler, J. L.; Johnson, M. R.; Lin, T.-Y.; Creager, S. E. *J. Am. Chem. Soc.* **1988**, *110*, 3659−3661.
(9) Sessler, J. L.; Johnson, M. R.; Creager, S. E.; Fettinger, J. C.; Ibers, J. A. *J. Am. Chem. Soc.* **1990**, *112*, 9310−9329.
(10) Sessler, J. L.; Capuano, V. L.; Harriman, A. *J. Am. Chem. Soc.* **1993**, *115*, 4618−4628.
(11) Gust, D.; Moore, T. A. *Science* **1989**, *244*, 35−41.
(12) Gust, D.; Moore, T. A.; Moore, A. L.; Gao, F.; Luttrull, D.; DeGraziano, J. M.; Ma, X. C.; Makings, L. R.; Lee, S.-J.; Trier, T. T.; Bittersmann, E.; Seely, G. R.; Woodward, S.; Bensassoon, R. V.; Rougée, M.; De Schryver, F. C.; van der Auweraer, M. *J. Am. Chem. Soc.* **1991**, *113*, 3638−3649.
(13) Gust, D.; Moore, T. A.; Moore, A. L.; Leggett, L.; Lin, S.; DeGraziano, J. M.; Hermant, R. M.; Nicodem, D.; Craig, P.; Seely, G. R.; Nieman, R. A. *J. Am. Chem. Soc.* **1993**, *97*, 7926−7931.
(14) Steinberg-Yfrach, G.; Liddell, P. A.; Hung, S.-C.; Moore, A. L.; Gust, D.; Moore, T. A. *Nature* **1997**, *385*, 239−241.
(15) Wasielewski, M. R. *Chem. Rev.* **1992**, *92*, 435−461.

10.1021/ja9939587 CCC: $19.00
Published on Web 07/11/2000

[(porphinato)zinc(II)] chromophores via metal-mediated cross-coupling chemistry in which the individual (porphinato)zinc(II) units are linked via cylindrically π-symmetric ethyne or butadiyne moieties at the *meso*- or β-positions of their respective macrocycles,[1,2,29,30] and demonstrated that controlling the nature of the porphyrin-to-porphyrin linkage topology provides an exquisite method to modulate the degree of both ground- and excited-state electronic coupling between pigments in multiporphyrin systems.[1,2,31,32]

Mechanistic studies of excitation transfer processes in multiporphyrin systems over nanosecond-to-picosecond time domains have typically required the syntheses of assemblies that feature spectroscopically identifiable chromophoric entities that function as energy donors and acceptors. The lowest excited singlet and triplet states of (porphinato)metal complexes are generally higher in energy than the analogous excited states of their respective free base porphyrin macrocycles; hence, in weakly coupled (porphinato)zinc(II)−spacer−porphyrin (PZn−Sp−PH_2) systems, energy transfer from an electronically excited (porphinato)zinc(II) complex to the free base chromophore is typically observed. The spacer moieties in these PZn−Sp−PH_2 energy transfer systems have utilized hydrogen-bonded cytosines,[33] flexible diphenylcarboxy,[34,35] and diphenylalkoxy chains,[36−40] as well as more rigid phenyl,[7,8,41] diphenylamide,[12,13,42] diphenylpolyyne and -polyene,[43] diphenylphenanthroline,[44,45] diphenylbipyridine,[45] diphenylacetylene,[3,4,24,41,46−50] and bis(phenylethynyl)arene[51,52] units, to connect the porphyrin-based pigments; energy delocalization between the porphyrinic components is negligible due to the weak electronic coupling afforded by these classes of pigment-to-pigment bridging moieties.

In biological light harvesting assemblies that facilitate ultrafast energy migration events, substantial interchromophore electronic interactions cause individual pigment molecules to cease to be electronically distinct,[53] despite the anisotropic nature of the protein environment and the variability in the chromophore conformational landscape.[54−57] With these facts in mind, we have sought to probe the dynamical processes relevant to strongly coupled multipigment systems that feature a small degree of electronic asymmetry between their constituent chromophoric building blocks. We have chosen *meso*-to-*meso* ethyne-bridged bis(porphyrin) complexes[1,2] as an archetypal bis(pigment) system that features substantial ground- and excited-state chromophore−chromophore coupling, and utilize PH_2 and PZn units to establish electronic asymmetry. While the nature of the initially prepared excited state and ultrafast dynamical processes inherent to complexes such as 5-[(10,20-bis[3″,5″-(di-*tert*-butyl)-phenyl]porphinato)zinc(II)]-5′-[10′,20′-bis[3″,5″-(di-*tert*-butyl)-phenyl]porphyryl]ethyne will be reported elsewhere, this study contrasts the photophysics and spectroscopy of the singlet and triplet excited states of this compound with its electronically symmetric analogues bis[(5,5′,-10,20-bis[3″,5″-(di-*tert* butyl)-phenyl]porphinato)zinc(II)]ethyne and bis[5,5′,-10,20-bis[3″,5″-(di-*tert*-butyl)phenyl]porphyryl]ethyne, and probes the relative roles played by the ethyne moiety and pyrrolic nitrogen protonation in determining the nature of the S_1 and T_1 states of these species over the nanosecond-to-miscrsecond time domain.

Experimental Section

Porphyrinic Compounds. Exemplary syntheses of ethyne-bridged porphyrin compounds and their key precursor molecules have been reported previously.[1,2,30] Detailed syntheses and characterization data for 5-bromo-10,20-bis[3′,5′-(di-*tert*-butyl)phenyl]porphyrin, [5-bromo-10,20-bis[3′,5′-(di-*tert*-butyl)phenyl]porphinato]zinc(II), [5-trimethylsilylethynyl-10,20-bis[3′,5′-(di-*tert*-butyl)phenyl]porphinato]zinc(II), 5,-

(16) Miller, J. S.; Epstein, A. J. *Angew. Chem., Int. Ed. Engl.* **1994**, *33*, 385−415.
(17) Arnold, D. P.; Manno, D.; Micocci, G.; Serra, A.; Tepore, A.; Valli, L. *Langmuir* **1997**, *13*, 5951−5956.
(18) Gregg, B. A.; Fox, M. A.; Bard, A. J. *J. Phys. Chem.* **1990**, *94*, 1586−1598.
(19) Kampas, F. J.; Yamashita, K.; Fajer, J. *Nature* **1980**, *284*, 40.
(20) LeCours, S. M.; Guan, H.-W.; DiMagno, S. G.; Wang, C. H.; Therien, M. J. *J. Am. Chem. Soc.* **1996**, *118*, 1497−1503.
(21) Priyadarshy, S.; Therien, M. J.; Beratan, D. N. *J. Am. Chem. Soc.* **1996**, *118*, 1504−1510.
(22) Karki, L.; Vance, F. W.; Hupp, J. T.; LeCours, S. M.; Therien, M. J. *J. Am. Chem. Soc.* **1998**, *120*, 2606−2611.
(23) Anderson, H. L.; Martin, S. J.; Bradley, D. D. C. *Angew. Chem., Int. Ed. Engl.* **1994**, *33*, 655−657.
(24) Wagner, R. W.; Lindsey, J. S.; Seth, J.; Palaniappan, V.; Bocian, D. *J. Am. Chem. Soc.* **1996**, *118*, 3996−3997.
(25) O'Keefe, G. E.; Denton, G. J.; Harvey, E. J.; Phillips, R. T.; Friend, R. H.; Anderson, H. L. *J. Chem. Phys.* **1996**, *104*, 805−811.
(26) Beljonne, D.; O'Keefe, G. E.; Hamer, P. J.; Friend, R. H.; Anderson, H. L.; Brédas, J. L. *J. Chem. Phys.* **1997**, *106*, 9439−9460.
(27) O'Neil, M. P.; Niemczyk, M. P.; Svec, W. A.; Gosztola, D.; Gaines, G. L., III; Wasielewski, M. R. *Science* **1992**, *257*, 63−65.
(28) Debreczeny, M. P.; Svec, W. A.; Wasielewski, M. R. *Science* **1996**, *274*, 584−587.
(29) DiMagno, S. G.; Lin, V. S.-Y.; Therien, M. J. *J. Am. Chem. Soc.* **1993**, *115*, 2513−2515.
(30) DiMagno, S. G.; Lin, V. S.-Y.; Therien, M. J. *J. Org. Chem.* **1993**, *58*, 5983−5993.
(31) Angiolillo, P. J.; Lin, V. S.-Y.; Vanderkooi, J. M.; Therien, M. J. *J. Am. Chem. Soc.* **1995**, *117*, 12514−12527.
(32) Kumble, R.; Palese, S.; Lin, V. S.-Y.; Therien, M. J.; Hochstrasser, R. M. *J. Am. Chem. Soc.* **1998**, *120*, 11489−11498.
(33) Harriman, A.; Magda, D. J.; Sessler, J. L. *J. Chem. Soc., Chem. Commun.* **1991**, 345−348.
(34) Anton, J. A.; Loach, P. A.; Govindjee, *Photochem. Photobiol.* **1978**, *28*, 235−242.
(35) Gonen, O.; Levanon, H. *J. Chem. Phys.* **1986**, *84*, 4132−4141.
(36) Brookfield, R. L.; Ellul, H.; Harriman, A.; Porter, G. *J. Chem. Soc., Faraday Trans. 2* **1986**, *82*, 219−233.
(37) Regev, A.; Galili, T.; Levanon, H. *Chem. Phys. Lett.* **1986**, *131*, 140−146.
(38) Davila, J.; Harriman, A.; Milgrom, L. R. *Chem. Phys. Lett.* **1987**, *136*, 427−430.
(39) Mataga, N.; Yao, H.; Okada, T.; Kanda, Y. *J. Chem. Phys.* **1989**, *131*, 473−480.
(40) Sen, A.; Krishnan, V. *Chem. Phys. Lett.* **1998**, *294*, 499−506.
(41) Yang, S. I.; Lammi, R. K.; Seth, J.; Riggs, J. A.; Arai, T.; Kim, D.; Bocian, D. F.; Holten, D.; Lindsey, J. S. *J. Chem. Phys. B* **1998**, *102*, 9426−9436.
(42) Gust, D.; Moore, T. A.; Moore, A. L.; Kang, H. K.; DeGraziano, J. M.; Liddell, P. A.; Seely, G. R. *J. Phys. Chem.* **1993**, *97*, 13637−13642.
(43) Osuka, A.; Tanabe, N.; Kawabata, S.; Yamazaki, I.; Nishimura, Y. *J. Org. Chem.* **1995**, *60*, 7177−7185.
(44) Chardon-Noblat, S.; Sauvage, J.-P.; Mathis, P. *Angew. Chem., Int. Ed. Engl.* **1989**, *28*, 593−595.
(45) Chambron, J.-C.; Heitz, V.; Sauvage, J.-P.; Pierre, J.-L.; Zurita, D. *Tetrahedron Lett.* **1995**, *36*, 9321−9324.
(46) Prathapan, S.; Johnson, T. E.; Lindsey, J. S. *J. Am. Chem. Soc.* **1993**, *115*, 7519−7520.
(47) Wagner, R. W.; Lindsey, J. S. *J. Am. Chem. Soc.* **1994**, *116*, 9759−9760.
(48) Seth, J.; Palaniappan, V.; Johnson, T. E.; Prathapan, S.; Linsey, J. S.; Bocian, D. F. *J. Am. Chem. Soc.* **1994**, *116*, 10578−10592.
(49) Seth, J.; Palaniappan, V.; Wagner, R. W.; Johnson, T. E.; Lindsey, J. S.; Bocian, D. F. *J. Am. Chem. Soc.* **1996**, *118*, 11194−11207.
(50) Strachan, J.-P.; Gentemann, S.; Seth, J.; Kalsbeck, W. A.; Lindsey, J. S.; Holten, D.; Bocian, D. F. *Inorg. Chem.* **1998**, *37*, 1191−1201.
(51) Kawabata, S.; Yamazaki, I.; Nishimura, Y.; Osuka, A. *J. Chem. Soc., Perkin Trans. 2* **1997**, 479−484.
(52) Jensen, K. K.; van Berlekom, S. B.; Kajanus, J.; Mårtensson, J.; Albinsson, B. *J. Phys. Chem. A* **1997**, *101*, 2218−2220.
(53) van Grondelle, R.; Dekker: J. P.; Gillbro, T.; Sundstrom, V. *Biochim. Biophys. Acta* **1994**, *1187*, 1−65.
(54) Deisenhofer, J.; Michel, H. *Science* **1989**, *245*, 1463−1473.
(55) McDermott, G.; Prince, S. M.; Freer, A. A.; Hawthronthwaite-Lawless, A. M.; Papiz, M. Z.; Cogdell, R. J.; Isaacs, N. W. *Nature (London)* **1995**, *374*, 517−521.
(56) Koepke, J.; Hu, X.; Muenke, C.; Schulten, K.; Michel, H. *Structure* **1996**, *4*, 581−597.
(57) Gudowska-Nowak, E.; Newton, M. D.; Fajer, J. *J. Phys. Chem.* **1990**, *94*, 5−5801.

15-bis(trimethylsilylethynyl)-10,20-diphenylporphyrin, [5,15-bis[3′,5′-(di-*tert*-butyl)phenyl]porphinato]zinc(II) (**1**), [5-ethynyl-10,20-bis[3′,5′-(di-*tert*-butyl)phenyl]porphinato]zinc(II) (**2**), 5,15-bis[3′,5′-(di-*tert*-butyl)phenyl]porphyrin (**4**), 5-ethynyl-10,20-bis[3′,5′-(di-*tert*-butyl)phenyl]porphyrin (**5**), 5,15-diethynyl-10,20-diphenylporphyrin (**6**), bis[(5,5′,-10,20-bis[3″,5″-(di-*tert*-butyl)phenyl]porphinato)zinc(II)]ethyne (**7**), 5-[(10,20-bis[3″,5″-(di-*tert*-butyl)phenyl]porphinato)zinc(II)]-5′-[10′,-20′-bis[3″,5″-(di-*tert*-butyl)phenyl]porphyryl]ethyne (**8**), and bis[5,5′,-10,20-bis[3″,5″-(di-*tert*-butyl)phenyl]porphyryl]ethyne (**9**) are available as Supporting Information.

Ground-State Absorption and Steady-State Emission Spectroscopy. Electronic spectra were recorded on an OLIS UV/vis/NIR spectrophotometry system that is based on the optics of a Cary 14 spectrophotometer. Fluorescence emission spectra were obtained using a Perkin-Elmer LS-50 luminescence spectrometer.

Electroabsorption Spectroscopy. The experimental procedure and the data reduction method have been described in detail elsewhere.[58] Briefly, electroabsorption experiments were performed at 77 K in neat 2-methyl tetrahydrofuran (2MTHF) glass with a retrofitted Cary-14 spectrophotometer featuring OLIS control software in a single beam mode. The electroabsorption cell (indium−tin oxide coated quartz plates; Kapton tape spacers) was 50 μm thick, as determined interferometrically in the near-infrared region with an empty cell. The field-dependent and independent transmittance signals were detected by a photomultiplier tube (Hamamatsu R928; near-UV and blue region) and a silicon photodiode (Hamamatsu S5591; red and near-infrared region). The small second-order Stark transmittance signal ($V_{2\omega}$) was detected after passage through a current-to-voltage converter with a digital lock-in amplifier (Stanford Research, SR 850) at the second harmonic of the field modulation frequency (ω), typically 220 Hz.

According to Liptay, for a rigid, isotropic sample the wavelength-dependent change in absorption, $\Delta A(\nu)$, is given by a linear combination of zeroth, first, and second derivatives of $A(\nu)$:[59]

$$\Delta A(\nu) = \left\{ A_x\ A(\nu) + \frac{B_x}{15hc}\ \frac{\nu \mathrm{d}[A(\nu)/\nu]}{\mathrm{d}\nu} + \frac{C_x}{30h^2c^2}\ \frac{\nu \mathrm{d}^2[A(\nu)/\nu]}{\mathrm{d}\nu^2} \right\} \cdot F_{\mathrm{int}}{}^2$$

where h is the Planck's constant, c is the speed of light, ν is the energy in wavenumbers, and F_{int} is the internal field experienced by the molecules.[60] The coefficients A_x, B_x, and C_x have been described in detail elsewhere.[61] Briefly, C_x gives information regarding $\Delta\mu_{12}$, B_x gives information regarding the polarizability change, $\Delta\alpha_{12}$, and A_x provides information about the changes in the transition moment polarizability and hyperpolarizability, respectively.

Time-Resolved Fluorescence Spectroscopy. Fluorescence lifetimes and time-resolved fluorescence anisotropy data were obtained at the Regional Laser and Biotechnology Laboratory (RLBL) at the University of Pennsylvania using a time-correlated single-photon counting (TC-SPC) apparatus that has been previously described;[62] instrument response = 25 ps fwhm. The samples were prepared in distilled, dry solvents and degassed by three freeze−pump−thaw cycles. The concentration of the solutions was adjusted to give 0.16−0.20 OD absorption at the excitation wavelength. Sample integrity was assessed by obtaining ground-state electronic spectra before and after laser irradiation. All compounds were photostable under the conditions of these experiments; no evidence of decomposition was ever observed. Data were analyzed using the Lifetime (RLBL)[62] program. Conditions for the time-resolved fluorescence anisotropy decay experiments were identical except that rotation polarization filters were used to alternatively select the parallel ($I_{||}$) and perpendicular ($I_{\perp}$) components of the emission.

EPR Spectroscopy. Electron paramagnetic resonance experiments were performed with a Brüker ESP 300E spectrometer. Intracavity illumination was performed directly through the front louvers with fiber optics obtained from Eska, Mitsubishi Corporation using a 150 W Kuda quartz-halogen illuminator with appropriate filtration of infrared radiation (Corning blue heat filter or 1 M $CuSO_4$). Temperatures were maintained utilizing an Oxford ESR 900 continuous flow liquid helium cryostat regulated with an Oxford ITC4 temperature controller. Frequencies were determined using a Hewlett-Packard 5350B microwave frequency counter. All experiments were conducted at microwave powers that ensured that resonance saturation did not occur. Spectra of the photoexcited triplet states of these complexes were obtained by subtracting a dark spectrum from the spectrum accumulated during illumination. No evidence of photodegradation of any of the samples was observed. Samples were checked spectrophotometrically after each EPR experiment to ensure compound integrity.

Transient Absorption Spectroscopy. Transient absorption spectra were obtained at RLBL using an instrument described previously.[63] The compounds were excited to the lowest triplet state via the first excited singlet state with 700 nm radiation obtained from a Q-switched Nd:YAG laser with a repetition rate of 10 Hz (1−5 mJ). Pump−probe delay times were varied from 1 ns to 5 ms using a Princeton Research digital delay generator. The samples were prepared in dry 10:1 toluene−pyridine solvent and degassed by 3 freeze−pump−thaw cycles. The concentrations of the solutions were adjusted to give 0.2−0.4 OD absorption at the excitation wavelength. Ground-state electronic spectra were recorded before and after laser irradiation to ensure that the porphyrins were photostable. No degradation of the samples was evident after the prolonged laser irradiation times dictated by these experiments.

Electronic Structure Calculations. Frontier orbital energies for the monomeric and bis(porphyrin) compounds, as well as for the peripherally unsubstituted porphyrin and (porphinato)zinc(II) complexes, were determined by using CAChe ZINDO with standard INDO-1 semiempirical parameters at a configuration interaction (CI) level of 20.[64] Molecular structure files were constructed by first assigning a dsp^2 (square planar) geometry to the central zinc atoms in the (porphinato)-zinc(II) complexes; (porphinato)zinc(II) and (5,10,15,20-tetraphenylporphinato)zinc(II) were constructed with D_{4h} symmetry, (5,15-diphenylporphinato)zinc(II), [5,15-diethynyl-10,20-diphenylporphinato)zinc-(II), and bis[(5,5′,-10,20,-diphenylporphinato)zinc(II)]ethyne were fashioned with D_{2h} symmetry, while (5-phenylporphinato)zinc(II) and [5-ethynyl-10,20-diphenylporphinato]zinc(II) were restricted to C_{2v} symmetry. Electronic structure calculations were performed on ZINDO-optimized geometrical structures in which the dihedral angle of the 10- and 20-*meso*-phenyl groups was adjusted to 90° with respect to the porphyrin least-squares plane. The convergence criteria for these Restricted Hartree−Fock (RHF) self-consistent field (SCF) calculations required the root-mean-square difference in the elements of the density matrix to be below 0.000001 on two successive SCF cycles. Once an optimized structure was obtained for a (porphinato)zinc(II) complex, that of its porphyrin analogue was generated by deletion of the central metal atom and optimizing the metrical parameters of the pyrrolic N−H bonds; the coordinates for the carbon−carbon framework obtained for the (porphinato)zinc(II) compound were not reoptimized. The results of these calculations were pictorially generated using an isosurface value of 0.04. Frontier molecular energies were also determined for bis[(5,5′,-10,20-di(*p*-neopentyl benzoate)porphinato)zinc(II)]ethyne using structural coordinates elucidated from X-ray crystallographic data;[65] INDO-1 semiempirical parameters, configuration interaction level, and calculation convergence criteria were identical with those for the electronic structure calculations carried out for the ZINDO-optimized geometrical structures.

(58) Karki, L.; Lu, H. P.; Hupp, J. T. *J. Phys. Chem.* **1996**, *100*, 15637−15639.

(59) Liptay, W. *Excited States*; Academic Press: New York, 1974; Vol. 1, pp 129−229.

(60) The internal field is the product of the externally applied local field correction factor. For a spherical cavity model, the correction factor (assuming a solvent continuum) is $3\epsilon/(2\epsilon + 1)$. The experimentally determined value of ϵ for 2-methyltetrahydrofuran glass is 4.0, which yields an estimated correction factor of 1.28.

(61) Boxer, S. G. *The Photosynthetic Reaction Center*; Academic Press: New York, 1993; Vol. 2, pp 179−220.

(62) Holtom, G. R. *SPIE Proc.* **1990**, *1204*, 2−12.

(63) Papp, S.; Vanderkooi, J. M.; Owen, C. S.; Holtom, G. R.; Phillips, C. M. *Biophys. J.* **1990**, *58*, 177−186.

(64) ZINDO software provided by CAChe Scientific (Beaverton, OR).

(65) Miller, D. C.; Shediac, R.; Carrol, P. J.; Therien, M. J. Manuscript in preparation.

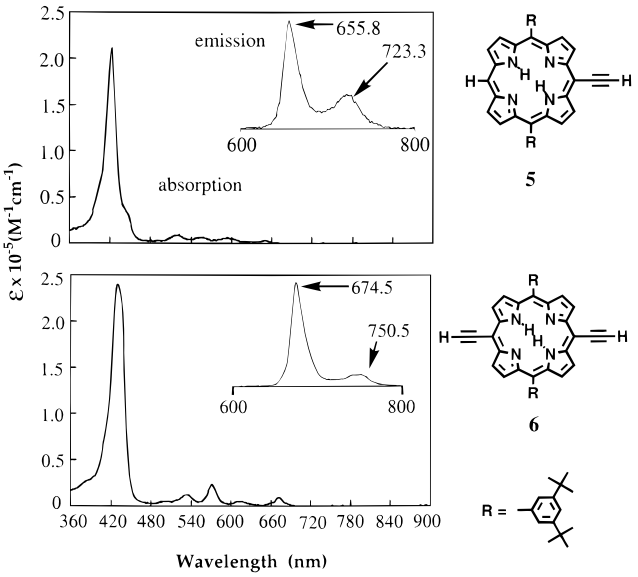

Figure 1. Room temperature electronic absorption and fluorescence emission spectra of compounds **5** and **6** in 10:1 toluene−pyridine solution.

Results and Discussion

(I) Steady-State Absorption and Emission Spectra. Absorption and fluorescence emission spectra were recorded in 10:1 toluene−pyridine for [5,15-bis[3′,5′-(di-*tert*-butyl)phenyl]-porphinato]zinc(II) (**1**), [5-ethynyl-10,20-bis[3′,5′-(di-*tert*-butyl)-phenyl]porphinato]zinc(II) (**2**), 5-phenylporphyrin (**3**), 5,15-bis[3′,5′-(di-*tert*-butyl)phenyl]porphyrin (**4**), 5-ethynyl-10,20-bis[3′,5′-(di-*tert*-butyl)phenyl]porphyrin (**5**), and 5,15-diethynyl-10,20-diphenylporphyrin (**6**). Spectra for monomeric (porphinato)-zinc(II) and porphyrin compounds **1**−**4** are available as Supporting Information, while those obtained for **5** and **6** are shown in Figure 1. Table 1 lists B- and Q-band absorption maxima with their relative extinction coefficients, as well as the observed fluorescence emission energies, for species **1**−**6**. As previously described for *meso*-ethynyl-substituted (porphinato)zinc(II) compounds,[1,2,66] appending π-conjugating ethynyl groups to the macrocycle *meso* positions shifts bathochromically the absorption maxima of the B- and Q-bands and introduces a disparity of oscillator strength between the *x*- and *y*-polarized $\pi \rightarrow \pi^*$ transitions; similarly, with respect to free base porphyrin (PH_2) species, increasing the degree of conjugation along the vector defined by the 5- and 15-*meso* positions (compounds **5** and **6**) complicates the optical spectra with respect to that evinced for benchmark PH_2 spectra (compounds **3**, **4**, and 5,10,15,20-tetraphenylporphyrin ($TPPH_2$)). Consistent with the Gouterman four orbital model,[67,68] expansion of π-conjugation at the *meso* position of porphine, the unsubstituted macrocycle, raises the filled a_u-derived orbital in energy while stabilizing the filled b_{1u}- and empty b_{2g}- and b_{3g}-derived molecular orbitals (vide infra). Accordingly, bathochromic shifts of the B- and Q-band absorption maxima are observed as the number of macrocycle *meso*-aryl substituents increases (**3** → **4** → $TPPH_2$). Larger magnitude B- and Q-band absorption maxima red shifts occur when *meso*-ethynyl substituents are appended to the porphyrin macrocycle (**4** → **5** → **6**) (Table 1). Broadening of the B band along the **4** → **5** → **6** series is observed (Table 2); the full width at half-maximum (fwhm) of these respective transitions varies from 731 to 992 to 1253 cm^{-1}. Furthermore, Gaussian deconvolution using simplex fitting methods of the B band of **6** reveals a 288 cm^{-1} splitting of the B_x and B_y states, whereas the B bands of compounds **4** and **5** can be mathematically fit with a single Gaussian function (data not shown). Because the absorbance ratio $[Q_x(0,0) + Q_y(0,0)]/[Q_x(1,0) + Q_y(1,0)]$ is a measure of the energetic degeneracy of free base porphyrin singlet excited-state configurations $[^1E(b_1,c_1) + {}^1E(b_1,c_2)]$ and $[^1E(b_2,c_1) + {}^1E(b_2,c_2)]$ (eq 1),[69,70] it is clear that as conjugation is

$$\frac{A(Q_x(0,0) + Q_y(0,0))}{A(Q_x(1,0) + Q_y(1,0))} = \text{constant}\{[^1E(b_1,c_1) + {}^1E(b_1,c_2)] - [^1E(b_2,c_1) + {}^1E(b_2,c_2)]\}^2 \quad (1)$$

augmented at the porphyrin 5 and 15 positions, the energy gap between the *x*- and *y*-polarized singlet transitions increases (compounds **4**, **5**, and **6**; Table 1). This is in accord with electronic structure calculations (vide infra), as well as with earlier work which explored how (porphinato)zinc(II) frontier orbital energies were perturbed as conjugation was expanded at the porphyrin 5- and 15-positions via ethyne moieties.[21,66]

A progressive red shift of the (0,0) and (0,1) components of the $S_1 \rightarrow S_0$ emission transitions is observed throughout the **3** → **4** → $TPPH_2$ and **4** → **5** → **6** chromophoric series (Table 1; Figure 1; Supporting Information). As conjugation is enhanced in compounds **4** → **5** → **6**, the emissive (0,0) transitions increase in intensity relative to their (0,1) counterparts (Figure 1; Supporting Information) while their respective Stokes shifts decrease (210 → 129 → 57 cm^{-1}), signifying that appending ethyne moieties to the porphyrin 5 and 15 positions effects increased nesting of the S_0 and S_1 potential energy surfaces. This observation bolsters the notions that an augmentation in conjugation along the axis defined by the 5- and 15-*meso*-carbon positions induces a rectangular distortion of the ground-state structure and causes the fluorescence emission to become progressively more polarized along this vector (vide infra). Furthermore, these effects are congruent with related electronic structural and dynamical studies of *meso*-arylethynyl-substituted (porphinato)metal complexes, which show that *meso*-arylethynyl moieties introduce an electronic structural perturbation that results in enhanced nonbonding character in the porphyrin-localized frontier orbitals relative to that observed in the parent macrocycle.[20−22,66,71]

The absorption and fluorescence emission spectra of the *meso*-to-*meso* bis(porphyrin) complexes **7**−**9**, measured in 10:1 toluene−pyridine solution at room temperature (Figure 2), differ dramatically from those of their component porphyrin monomers (see Figure 1; Supporting Information). While the data displayed in Figure 2 for these compounds bear marked similarity to the previously described electronic spectral features of bis[(5,5′,-10,20-diphenylporphinato)zinc(II)]ethyne,[1,2] it is important to note that in contrast to classic PZn−Sp−PH_2 systems, which exhibit absorption spectra that are essentially a superposition of their constituent monomers due to the weak porphyrin−porphyrin electronic coupling afforded by their respective spacer moieties,[3,7,8,13,34−36,38,39,43,48,49,51] compound **8** exhibits optical features that are characteristic of a bis(pigment) complex that features strong ground- and excited-state electronic coupling.[1,2] The fwhm of the B-band regions of ethyne-bridge bis(porphyrin)

(66) LeCours, S. M.; DiMagno, S. G.; Therien, M. J. *J. Am. Chem. Soc.* **1996**, *118*, 11854−11864.
(67) Gouterman, M. *J. Mol. Spectrosc.* **1961**, *6*, 138−163.
(68) Gouterman, M. *The Porphyrins*; Academic Press: London, 1978; Vol. III, pp 1−165.
(69) Spellane, P. J.; Gouterman, M.; Antipas, A.; Kim, S.; Liu, Y. C. *Inorg. Chem.* **1980**, *19*, 386−391.
(70) Perrin, M. H.; Gouterman, M.; Perrin, C. L. *J. Chem. Phys.* **1969**, *50*, 4137−4150.

Table 1. Prominent Absorption and Emission Bands for Complexes **1**−**9**[a]

	electronic absorptions, B-band region			electronic absorptions, Q-band region			fluorescent emission	
compd	λ (nm)	υ (cm^{-1})	[log(ϵ)]	λ (nm)	υ (cm^{-1})	[log(ϵ)]	λ (nm)	υ (cm^{-1})
TPPZn	428.7	23 324	(6.05)	561.3	17 816	(4.25)	603.0	16 584
				602.0	16 611	(3.95)	652.5	15 326
$TPPH_2$	415.5	24 067	(5.61)	512.9	19 497	(4.15)	652.5	15 326
				546.5	18 298	(3.62)	720.0	13 889
				591.0	16 920	(3.36)		
				649.3	15 401	(3.34)		
1	419.4	23 844	(5.41)	550.4	18 169	(3.98)	595.8	16 784
				586.8	17 042	(3.36)	646.5	15 468
2	427.5	23 392	(5.45)	563.2	17 756	(4.16)	615.4	16 250
				605.2	16 523	(3.84)	670.8	14 908
3	399.2	24 882	(5.17)	496.4	20 145	(3.88)	626.5	15 962
				526.1	19 008	(2.96)	686.5	14 567
				567.9	17 609	(3.43)		
				619.2	16 150	(2.54)		
4	408.6	24 474	(5.28)	504.5	19 822	(3.91)	639.9	15 627
				538.2	18 580	(3.50)	698.1	14 325
				576.0	17 361	(3.48)		
				631.4	15 837	(3.14)		
5	422.1	23 691	(5.32)	519.3	19 257	(4.49)	655.8	15 249
				554.4	18 038	(4.25)	723.3	13 826
				593.6	16 846	(4.03)		
				650.3	15 378	(3.82)		
6	430.2	23 245	(5.38)	531.5	18 815	(4.11)	674.5	14 826
	435.6	22 957	(5.35)	572.0	17 483	(4.37)	750.5	13 324
				611.1	16 364	(3.72)		
				671.9	14 883	(3.99)		
7	415.4	24 073	(4.7)	555.8	17 992	(3.8)	732.7	13 648
	434.3	23 026	(4.6)	708.3	14 118	(4.3)		
	447.8	22 331	(4.5)					
	482.9	20 708	(5.1)					
8	411.3	24 313	(4.6)	526.1	19 008	(3.8)	734.4	13 617
	426.2	23 463	(4.7)	569.3	17 565	(3.8)		
	476.1	21 004	(4.8)	650.3	15 378	(4.0)		
				712.4	14 037	(4.2)		
9	404.6	24 716	(5.1)	515.3	19 406	(4.4)	716.0	13 966
	424.8	23 540	(5.1)	612.5	16 327	(4.4)		
	470.7	21,245	(5.2)	707.0	14,144	(4.5)		

[a] All spectra recorded in 10:1 toluene−pyridine

Table 2. Comparative Absorptive Domains of the Blue and Red Spectral Regions of Compounds **1**−**9**[a]

compd	fwhm[b] B-band region [cm^{-1}]	fwhm[c] Q-band region [cm^{-1} (nm)]	compd	fwhm[b] B-band region [cm^{-1}]	fwhm[c] Q-band region [cm^{-1} (nm)]
TPPZn	486	663 (561.3)	**5**	992	1201 (519.3)
		470 (602.0)			889 (554.4)
					1044 (593.6)
					678 (650.3)
$TPPH_2$	706	856 (512.9)	**6**	1253	940 (531.5)
		636 (546.5)			522 (572.0)
		653 (591.0)			1044 (611.1)
		331 (649.3)			678 (671.9)
1	574	835 (550.4)	**7**	4439	1882 (555.8)
		627 (586.8)			1305 (708.3)
2	783	888 (563.2)	**8**	4700	1305 (569.3)
		887 (605.2)			2193 (712.4)
3	888	888 (496.4)	**9**	4908	1880 (612.5)
		574 (567.9)			1097 (707.0)
4	731	888 (504.5)			
		636 (538.2)			
		601 (576.0)			
		321 (631.4)			

[a] From electronic spectra recorded in 10:1 toluene−pyridine. [b] Taken as the spectral width of the B-band region at half the height of the most intense absorption. [c] Entries correspond to the spectral window centered about the electronic transition in parentheses. See Figures 1−2 and Supporting Information.

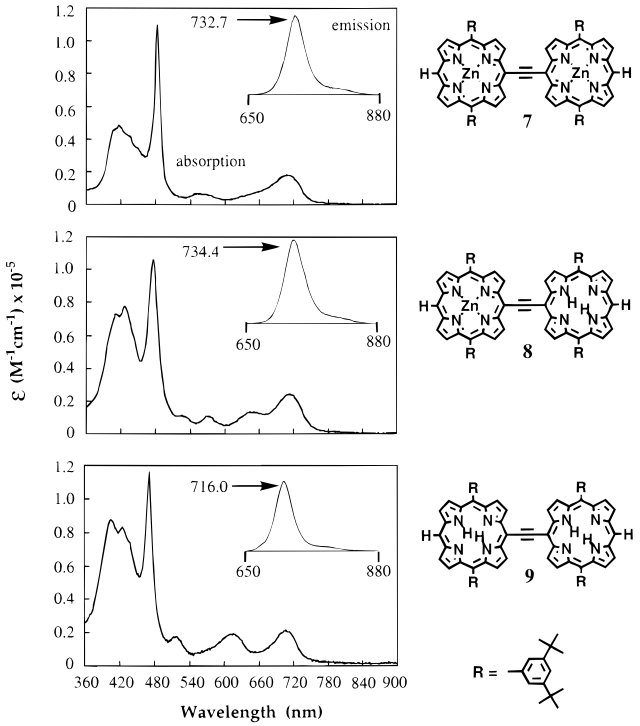

Figure 2. Room temperature electronic absorption and fluorescence emission spectra of compounds **7**, **8**, and **9** in 10:1 toluene−pyridine solution.

systems **7**, **8**, and **9** are 4439, 4699, and 4908 cm^{-1}, respectively (Table 2); note also that the energy separations between the two sharp transitions that lie at opposite extremes of these respective B-band envelopes are substantial [**7** (3365 cm^{-1}), **8** (3309 cm^{-1}), **9** (3471 cm^{-1})]. Interestingly, although the symmetry of PH_2 (D_{2h}) is reduced with respect to PZn (D_{4h})

and porphyrin and (porphinato)metal chromophores have nonsuperimposable molecular symmetry axes, a similar vectorial arrangement of the *x*- and *y*-polarized transition dipoles (*x*-axis defined as the molecular axis of highest conjugation) in bis(porphyrin) complexes **7**−**9** can be inferred from the high degree of correspondence between their respective B-band splitting patterns. This supposition is in fact consistent with experimental data obtained from fluorescence anisotropy studies and electronic structure calculations (vide infra). On the basis of X-ray crystallographic studies,[65] solid-state and low-temperature optical spectroscopic data,[65] and transient fluorescence anisotropy measurements[32] of *meso*-to-*meso* ethynyl-linked (porphinato)zinc(II) systems, the spectral heterogeneity of the low-energy Q_x absorption band of **7** can be partly ascribed to the presence of a distribution of ground-state conformers in solution; the dominant, lowest energy component of this envelope corresponds to a maximally conjugated structure in which the two component PZn units are approximately coplanar, while the higher energy components of the Q_x band have either a vibronic genesis or derive from electron excitation of a population of nonplanar structural conformers. The additional electronic perturbation afforded by the PH_2 units complicates the low-energy region of the optical spectrum of **8** and **9** relative to **7**. Gaussian deconvolution of the low-energy absorbance features of **7**, **8**, and **9** using standard simplex fitting methods reveal low energy, high oscillator strength transitions centered at 14060, 14022, and 14162 cm^{-1}, respectively, that dominate this region of the Q-state absorption band envelope (data not shown). Approximately 800 cm^{-1} to the blue of these transitions lies a higher energy *x*-polarized state[32,65] in compounds **7**−**9**; based on analogy to spectroscopic data obtained in closely related systems,[32] these bands likely have their genesis in the fact that significant conformational heterogeneity is manifest for these compounds in solution at ambient temperature. The integrated oscillator strengths of the two lowest energy *x*-polarized Q states thus reflect the relative populations of two families of conformers that differ with respect to the extent of porphyrin−porphyrin conjugation. The highest energy component of the Q_x absorption band envelope of these species is separated by a standard porphyrinic vibronic spacing (∼1600 cm^{-1})[68] from the lowest energy *x*-polarized Q state.

The magnitude of the Stokes shift, determined by using the lowest energy transition from deconvoluted spectra, is small in compounds **7**, **8**, and **9** (412, 405, and 196 cm^{-1} respectively); these data indicate that electronically asymmetric **8** is not subject to excited-state nuclear distortions appreciably different than that experienced by **7** and **9** in the excited singlet state. Congruently, the marked correspondence of both emission band shapes and energies in compounds **7**−**9** (Figure 2 and Table 1) suggest that the nature of their S_1 excited states is similar. While small differences in the emission wavelengths of these complexes may derive from axial ligation effects that raise the a_{2u}-derived orbitals of the PZn units, or minor charge resonance effects which lower marginally the energy of **8**'s S_1 state with respect to that for compounds **7** and **9**, the absorption and emission data obtained for **7**−**9** emphasize that relative to the differences in electronic structure that exist between PH_2 and PZn building blocks, the electronic perturbation to the frontier orbitals that derives from the existence of the *meso*-to-*meso* ethyne bridge is extreme. The cylindrically π-symmetric porphyrin-to-porphyrin linker thus constitutes the primary determinant of the nature of the S_1 excited state, and the redistribution of electron density that accompanies the S_0-S_1 transition for these bis(porphyrin) chromophores.

Table 3. Photophysical Properties of S_1 Excited States of Porphyrin Compounds **4**−**9**: Fluorescence Lifetime and Time-Resolved Anisotropy Data[a−d]

compd	λ_{ex} (nm)	λ_{em} (nm)	τ_f (ns)	r_0 (at 20 ps)	τ_r (ns)
$TPPH_2$	637	725	12.1	0.4	0.12
4	631	670	11.3	0.4	0.12
5	650	670	11.7	0.2	0.12
6	665	680	10.1	0.3	0.16
7	704	720	1.2	0.4	0.33
8	704	720	1.9	0.4	0.34
9	704	720	3.1	0.4	0.33

[a] Samples were kept rigorously dry using standard inert-atmosphere techniques; all data presented were recorded at 293 K in 10:1 toluene−pyridine. [b] The fluorescence lifetimes were determined using a time-correlated single-photon counting (TCSPC) apparatus (Regional Laser and Biotechnology Laboratory, University of Pennsylvania) that has been previously described.[62] Instrument response function: 25 ps fwhm. Data were analyzed using the Lifetime (RLBL) program. [c] Time-resolved anisotropy decay data were obtained using rotating polarization filters to alternatively select the parallel and perpendicular components of the emission; all other experimental conditions were identical with those of the lifetime measurements. [d] τ_F = fluorescence lifetime; r_o = initial fluorescence anisotropy determined 20 ps after excitation; τ_r = rotational diffusional time constant.

(II) Excited Singlet State Dynamics: Time-Resolved Fluorescence Lifetime and Anisotropy Studies. The magic angle and anisotropic dynamics of the S_1 states of **4** → **9** were investigated in 10:1 toluene−pyridine using time-correlated single photon counting. The bis(porphyrin) complexes were all optically pumped on the red side of the lowest energy absorption. Monoexponential singlet state lifetimes (τ_F) were observed for **7**, **8**, and **9** that ranged between 1 and 3 ns (Table 3). While these τ_F values are of similar magnitude to those observed for simple (porphinato)zinc(II) complexes, it is interesting to note that the fluorescence lifetime of compound **9** is diminished with respect to that seen for *meso*-arylporphyrins ($\tau_F \approx 11$ ns, Table 3), indicating an enhancement of intersystem crossing and/or nonradiative decay pathways from the S_1 state in this species relative to standard porphyrin chromophores.

The fluorescence anisotropy $r_{(t)}$ is obtained from the parallel ($I_{||}$) and perpendicular ($I_\perp$) transient signals using the following expression:[72]

$$r_{(t)} = \frac{I_{||}(t) - I_\perp(t)}{I_{||}(t) + 2I_\perp(t)} \qquad (2)$$

After deconvolution of the instrument response function, values for the initial anisotropy r_0 ($t = 20$ ps) were observed by fitting the anisotropy decay $r(t)$ to a single exponential, $r(t) = r_0 e^{(-t/\tau_r)}$, where τ_r is the rotational diffusion time constant. The benchmark (porphinato)zinc(II) complex, (5,10,15,20-tetraphenylporphinato)zinc(II) (TPPZn), possesses a doubly degenerate S_1 excited state displaying an initial anisotropy $r_0 = 0.1$ ($t = 20$ ps) following electronic excitation on the red edge of the lowest energy Q transition.[32] The measured value of the initial anisotropy ($r_0 = 0.2$; $t = 20$ ps) for both (5-trimethylsilylethynyl-10,20-diphenylporphinato)zinc(II) and [5,15-bis(trimethylsilylethynyl)-10,20-diphenylporphinato]zinc(II)[32,73] shows that expansion of porphyrin conjugation via *meso*-ethynyl moieties introduces an electronic perturbation sufficient to cause a splitting of the *x*- and *y*-polarized transitions.[32,73] For the

(71) LeCours, S. M.; Phillips, C. M.; de Paula, J. C.; Therien, M. J. *J. Am. Chem. Soc.* **1997**, *119*, 12578−12589.
(72) Lakowicz, J. R. *Principles of Fluorescence Spectroscopy*; Plenum Press: New York, 1983,
(73) Lin, V. S.-Y. Ph.D. Thesis, University of Pennsylvania, Philadelphia, 1996.

5-ethynyl and 5,15-diethynyl derivatives of 10,20-diphenylporphyrin (**5** and **6**), the measured values of the initial anisotropy ($t = 20$ ps) are 0.2 and 0.3, respectively; this contrasts the value of 0.4 obtained for the initial fluorescence anisotropy of **4** and $TPPH_2$, as expected for simple porphine derivatives which possess singly degenerate excited states. These data indicate that the transition dipole of the lowest energy S_1 excited state of compounds of **5** and **6** is no longer polarized along the vector that bisects the pair of proton-bearing nitrogen atoms in the macrocycle core. The orientation of orthogonal *x*- and *y*-polarized excited states for **5** and **6** has changed with respect to that seen for simple free-base porphyrin chromophores, rotating in the porphyrin principal axis system toward the *meso*-carbon positions that bear the ethyne substituents. Moreover, the fluorescence anisotropy data indicate that compounds **5** and **6** possess a smaller energy gap between their Q_x and Q_y states than does porphine. The anisotropy value of 0.2 observed for compound **5** shows dramatically the degree to which a single *meso*-ethynyl substituent perturbs the porphine frontier orbitals, driving the *x*- and *y*-polarized Q states to near energetic degeneracy. The fluorescence anisotropy decays can be fit as a single exponential for all of these monomeric porphyrins, with the rotational depolarization time τ_r in the range 120−160 ps (Table 3).

The value of the initial fluorescence anisotropy ($r_0 = 0.4$, $t = 20$ ps) for compounds **7**, **8**, and **9** (Table 3) confirms a singly degenerate S_1 excited state for these bis(porphyrin) complexes, consistent with an energetic splitting of the *x*- and *y*-polarized S_1 states that is sufficiently large to suppress *x*- and *y*-polarized excited-state population exchange on the time scale of these measurements. These time-resolved fluorescence anisotropy studies thus show that like bis[(5,5′,-10,20-diphenylporphinato)-zinc(II)]ethyne,[32,73] conjugated bis(porphyrin) complexes **7**−**9** possess low-energy emitting states polarized along the long (*x*) axis of the molecule. Compounds **7**, **8**, and **9** exhibit single-exponential fluorescence anisotropy decay time constants with τ_r values in the range of 330−340 ps (Table 3). Note that the τ_r values obtained for the bis(porphyrin) systems are roughly twice that of those measured for monomeric species **4**−**6**, consistent with the fact that the magnitude of the rotational depolarization time constant tracks with molecular size.[72]

A highly polarized S_1 excited state distinguishes *meso*-to-*meso* ethyne-bridged porphyrin compounds **7**−**9** from other classes of bis(porphyrin) complexes; this is especially evident in the S_1-state dynamics exhibited by **8**, which contrasts the photophysical behavior observed for conventional covalently linked PZn−Sp−PH_2 assemblies[3,7,12,13,34,36,38−41,43,44,48−52] which are dominated by energy transfer from the PZn unit to the PH_2 moiety and the deactivation processes inherent to the PH_2-localized singlet excited state. The fact that the polarized, singly degenerate nature of the S_1 state of *meso*-to-*meso* ethyne-bridged **7** is also manifest in compounds **8** and **9** shows that (i) the electronic perturbation induced by conjugation expansion mediated by the ethyne moiety exceeds significantly that which derives from the electronic asymmetry of the PH_2 macrocycle pyrrole rings and (ii) moderate differences between the energies and symmetries of the frontier orbitals of the monomeric pigment building blocks of *meso*-to-*meso* ethyne-linked porphyrin arrays neither cause S_1 state excitation localization nor reduce the degree of excited-state polarization. Hence, this conjugated, multiporphyrin structural motif offers considerable engineering flexibility to develop synthetic assemblies that effect long-range, high-quantum yield, vectorial energy migration reactions reminiscent of the biological light-harvesting complexes.[53]

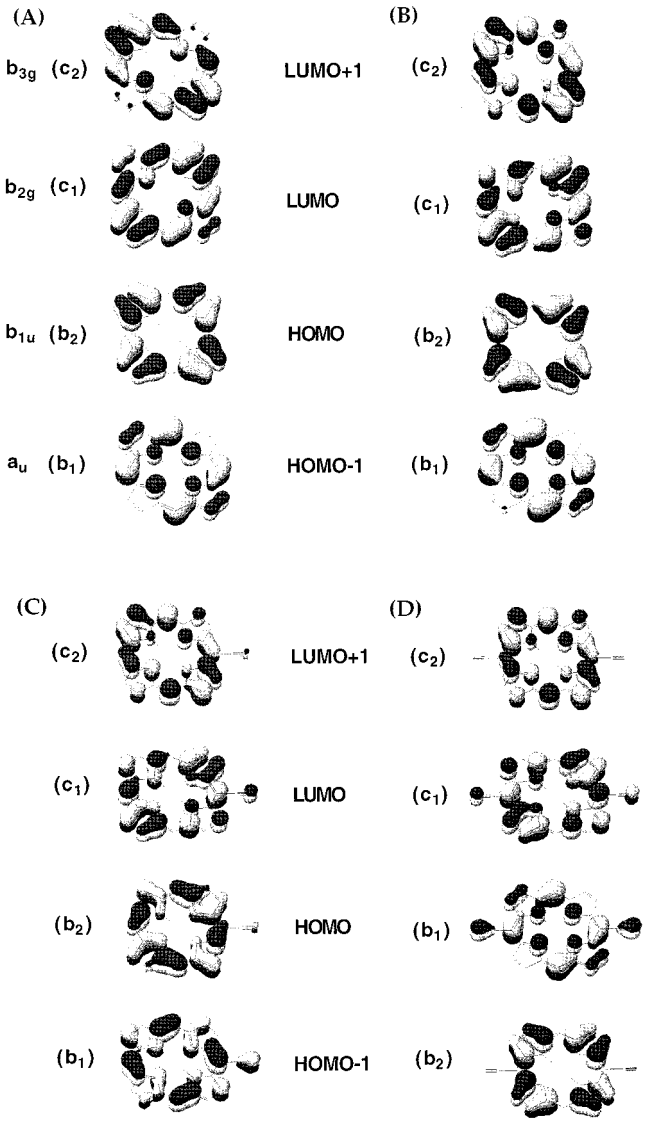

Figure 3. Frontier molecular orbitals of (A) porphine, (B) 5,15-diphenylporphyrin, (C) 5-ethynyl-10,20-diphenylporphyrin, and (D) 5,-15-diethynyl-10,20-diphenylporphyrin. Electron density localized on *meso*-aryl rings has been omitted for clarity.

(III) Electronic Structure Calculations. Spectroscopic and computational studies have shown that *meso*-aryl-ethynyl substituents significantly perturb frontier orbital (FO) energies of (porphinato)zinc(II) complexes, resulting in large energy separations between the formerly degenerate (porphinato)metal *x*- and *y*-polarized excited states.[21,66,71] Similarly, electronic structure calculations carried out using semiempirical methods (configuration interaction level = 20; see Experimental Section for details) show that relative to porphine (Figure 3A), the corresponding frontier orbitals (FO's) determined for *meso*-ethyne elaborated **5** and **6** (Figure 3, parts C and D, respectively) manifest substantive electronic differences relative to porphyrin macrocycles bearing more conventional aryl substituents (**3,** Figure 3B).[74] Note that the porphine b_1 orbital becomes progressively destabilized with augmented conjugation at the macrocycle periphery (Table 4) while the corresponding b_2 orbital becomes increasingly stabilized across the **PH_2** to **4** to **5** to **6** series; this trend ultimately results in a b_1 highest occupied molecular orbital (HOMO) for diethynyl-derivatized **6**, and a

Table 4. Calculated Frontier Orbital Energies (eV) of Compounds **3**−**6** and Benchmark PH_2 and PZn Species and of Ethyne-Bridged Bis(porphyrin) Complexes **7**−**9** and Benchmark PZn Monomers **1** and **2**

A. Compounds **3**−**6** and Benchmark PH_2 and PZn Species

	complex						
orbital	PZn(II)	PH_2	**3**	**4**	$TPPH_2$	**5**	**6**
LUMO+3	1.650	1.217	0.792	0.792	0.800	0.782	0.761
LUMO+2	0.491	0.272	0.244	0.244	0.250	0.160	0.053
LUMO+1	−1.215	−1.345	−1.265	−1.330	−1.131	−1.374	−1.429
LUMO	−1.215	−1.448	−1.440	−1.508	−1.329	−1.565	−1.652
HOMO	−6.344	−6.315	−6.551	−6.364	−6.513	−6.427	−6.400
HOMO−1	−6.895	−6.699	−6.771	−6.561	−6.653	−6.463	−6.499
HOMO−2	−9.077	−8.457	−8.436	−8.434	−8.442	−8.473	−8.473
HOMO−3	−9.078	−8.605	−8.579	−8.576	−8.475	−8.545	−8.566

B. Ethyne-Bridged Bis(porphyrin) Complexes **7**−**9** and Benchmark PZn Monomers **1** and **2**

	complex					
orbital	**1**	**2**	**7**	**8**	**9**	**7′** (crystal structure)
LUMO+3	1.041	1.031	−1.132	−1.147	−1.394	−0.836
LUMO+2	0.461	0.371	−1.180	−1.163	−1.400	−0.871
LUMO+1	−1.170	−1.204	−1.190	−1.221	−1.402	−0.946
LUMO	−1.304	−1.377	−1.635	−1.589	−1.958	−1.267
HOMO	−6.402	−6.477	−6.279	−6.174	−6.233	−5.845
HOMO−1	−6.717	−6.590	−6.434	−6.431	−6.491	−6.171
HOMO−2	−8.721	−8.681	−6.446	−6.704	−6.503	−6.228
HOMO−3	−8.759	−8.719	−6.908	−6.875	−6.842	−6.437

small energy gap between the HOMO and HOMO-1 relative to that determined for porphine. Appending ethyne moieties to the porphine 5 and 15 positions stabilizes both the unoccupied c_1 and c_2 orbitals with respect to the parent macrocycle. Because the net stabilization of the c_1 orbital of **5** and **6** relative to the porphine c_1 is greater than that observed for the corresponding c_2 orbitals, the LUMO-LUMO+1 energy separation in *meso*-ethynyl elaborated **5** and **6** exceeds that for PH_2. The average energy of the HOMO and HOMO-1 orbitals signals that the filled FOs of **5** and **6** are only stabilized slightly (∼0.05 eV) with respect to the average energy of the analogous orbitals of PH_2; this contrasts the case for the unfilled c_1- and c_2-derived orbitals. Note that the average energy of the two low-lying empty orbitals of **5** and **6** drops considerably (0.07 and 0.14 eV, respectively) with respect to that calculated for porphine, and hence is the primary factor responsible for the narrowing of the S_0-S_1 optical band gap that is manifest when cyllindrically π-symmetric ethyne moieties are fused directly to the macrocycle 5- and 15-*meso*-carbon positions.

Note that the four Gouterman orbitals of **5** as well as the HOMO and LUMO of **6** possess appreciable electron density along the vector defined by the ethynyl moieties (Figure 3). The frontier orbitals of **5** and **6** determined from INDO electronic structure calculations are thus consistent with our pump−probe fluorescence anisotropy experiments (vide supra), which indicated that a reorientation of the *x*- and *y*-polarized Q states had occurred relative to PH_2 and that the lowest energy S_1-excited states of **5** and **6** were no longer polarized along the molecular symmetry axis defined by the two protonated pyrrolic nitrogens.

To obtain insight into how PH_2 chromophoric components impact the optoelectronic properties of compounds **8** and **9** with respect to that elucidated for the *meso*-to-*meso* ethyne-bridged bis(porphinato)zinc(II) complex **7**,[1,2,32,74] we performed electronic structure calculations using standard INDO-1 semiempirical parameters (CI = 20) to determine the respective FO energies and electron density distributions for these three bis(porphyrin) complexes. Bis(porphyrin) structures featuring planar macrocycles constrained to lie in a common molecular plane were utilized as optimized geometries for **7**, **8**, and **9**. The FOs of these species are shown in Figure 4 and their calculated energies are listed in Table 4. The most salient feature in the frontier orbital sets for **7**−**9** (Figure 4A−C) is the ethynyl-bridge-localized electron density apparent in the HOMO and LUMO. Accordingly, the magnitude of the LUMO-LUMO+1 splitting is dramatically enhanced in **7**, **8**, and **9** (0.445, 0.379, and 0.350 eV, respectively) relative to benchmark chromophores [PZn (0.0 eV), PH_2 (0.103 eV), **1** (0.134 eV), and **4** (0.178 eV)], as well as to their constituent ethyne-substituted, monomeric building blocks **2** (0.173 eV), **5** (0.191 eV), (5,15-diethynyl-10,20-diphenylporphinato)zinc(II) (0.232 eV, Supporting Information), and **6** (0.223 eV) (Table 4).

The HOMOs of bis(porphyrin) compounds **7**, **8**, and **9** exhibit significant electron density at the ethynyl bridge, the macrocycle 5- and 5′-*meso*-carbon positions, and the C_α-carbon atoms bonded to these two C_{meso} atoms. It is noteworthy that relative to the filled a_{2u} symmetric FO of (porphinato)zinc(II) compounds or the b_1 orbitals of simple porphyrin macrocycles to which the HOMOs of **7**, **8**, and **9** can trace their genesis, the HOMOs of the *meso*-to-*meso* ethyne-bridged bis(porphyrin) complexes exhibit a number of interesting electronic structural perturbations. While the highest energy filled orbitals of **7**, **8**, and **9** retain the substantial C_{meso}- and N-centered electron density of PZn- or PH_2-derived a_{2u}/b_1 orbitals, they also display substantially reduced electron density at the C_α and C_β carbon atoms, as well as enhanced nonbonding character with respect to the analogous orbitals of their monomeric porphyrin counterparts. Note also that in **7**, **8**, and **9**, only the two C_{meso} atoms that constitute a portion of the conjugated porphyrin-to-porphyrin bridge exhibit substantial π overlap with their respective C_α carbons; the C_{meso} carbons that lie at the extrema of the conjugated axis (the 15- and 15′-positions) of these bis(porphyrin) compounds are essentially nonbonding with respect

(74) To simplify our discussion of the respective frontier orbital energies and electron density distributions determined for $TPPH_2$, **4**, **5**, and **6**, we use the orbital labeling convention established by Gouterman.[69,70] Hence, the a_u-, b_{1u}-, b_{2g}-, and b_{3g}-symmetric orbitals of porphine (Figure 5A) bear the respective b_1, b_2, c_1, and c_2 labels; these labels are retained as symmetry is reduced from D_{2h} in compounds **4**, **5**, and **6**.

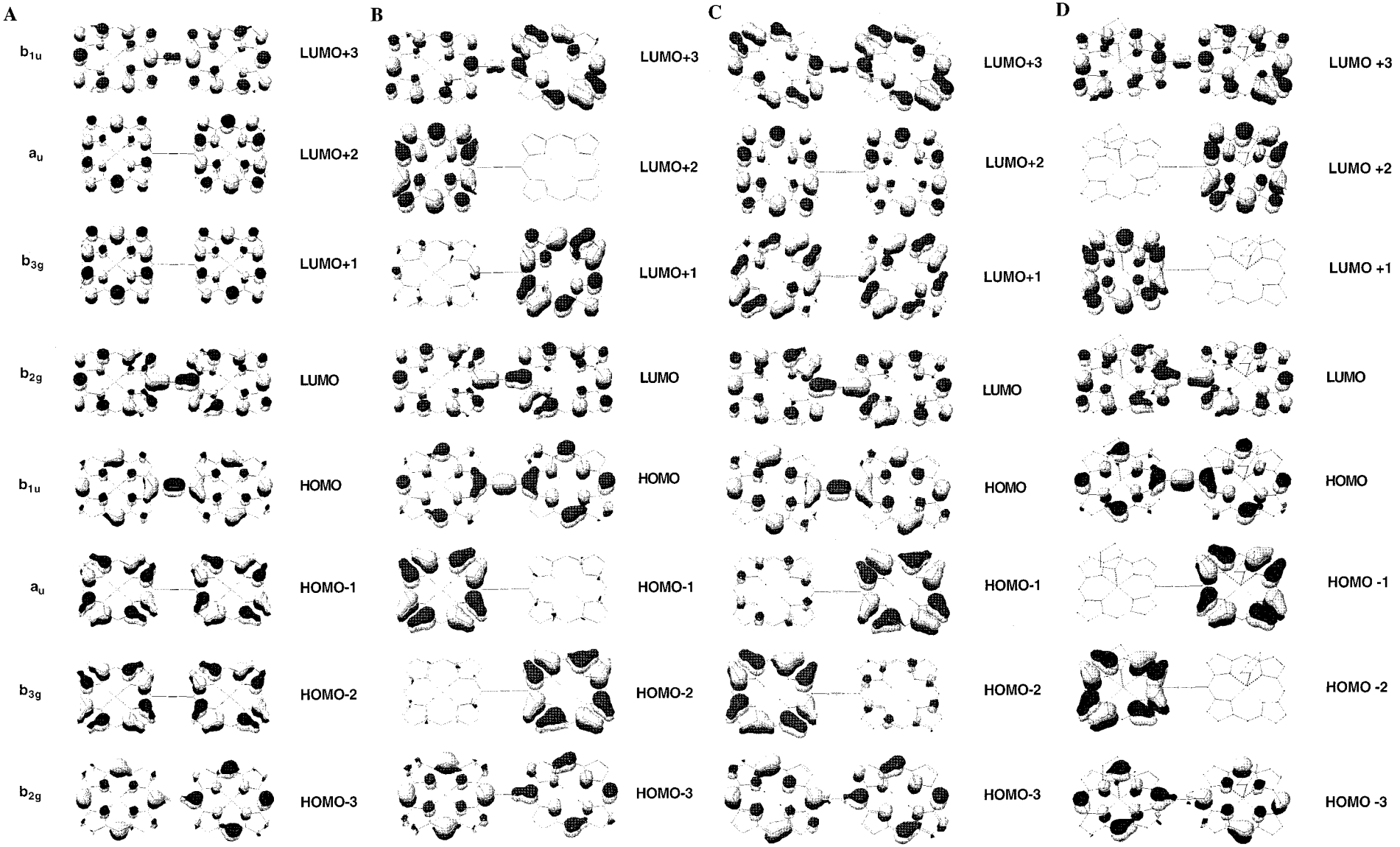

Figure 4. Frontier molecular orbitals of bis(porphyrin) compounds (A) **7,** (B) **8,** (C) **9,** and (D) bis[(5,5′,-10,20-di(*p*-neopentyl benzoate)porphinato)zinc(II)]ethyne (**7′**). The nuclear coordinates utilized for **7**, **8**, and **9** correspond to those obtained for computationally optimized structures, while those for **7′** were determined from an X-ray crystallographic study (see text for details). Electron density localized on *meso*-aryl rings has been omitted for clarity.

to their neighboring C_α atoms, while the four C_{meso} carbons that lie orthogonal to the conjugated axis exhibit appreciable π overlap with only a single C_α carbon. Relative to the electron density distributions observed for the PZn a_{2u} and PH_2 b_1 orbitals, the HOMOs of **7**, **8**, and **9** show substantially diminished $C_\beta-C_\beta$ in-phase orbital interactions, as well as reduced $C_\alpha-N$ antibonding character.

The LUMOs of compounds **7**−**9** possess extensive cumulenic character, displaying both in-phase orbital interactions involving the carbon atoms of the ethynyl moiety that are bound directly to porphyrin macrocycle *meso*-carbon atoms and diminished bond order between the ethyne carbons, consistent with both an earlier analysis of the optical spectra of this class of chromophores[1,2] and an extensive body of spectral and computational data obtained for related [5,15-bis[(aryl)ethynyl]-porphinato]metal complexes.[20−22,66,71] No electron density is apparent at the 10(10′)- and 20(20′)-*meso*-carbon positions in the LUMOs of these complexes; furthermore, pyrrole-localized electron density in the PH_2 units of **8** and **9** is diminished in these orbitals with respect to that seen in the LUMOs of PH_2-derived compounds **3**−**6**. Both the electron density distributions in the frontier orbital set and the magnitude of the energy separation between these orbitals in compounds **7**, **8**, and **9** are consistent with the fluorescence anisotropy data which evinced that the S_1 emitting state is polarized exclusively along the molecular axis defined by the ethyne bridge.

Despite differences in symmetry [**7** (D_{2h}), **8** (C_s), **9** (C_s)] and the electronic structures of their respective porphyrinic components, there exists distinct similarities in the FO electron density distributions and energies of species **7**−**9**, underscoring the pivotal role of the ethyne moiety in determining the nature of the ground and excited states of these compounds. The stabilization apparent in the low-lying antibonding levels of **7**−**9** relative to those calculated for simple, unelaborated PH_2 and PZn systems is a manifestation of the extension of π conjugation (Table 4); a similar effect has been observed for simple [5,15-bis[(aryl)ethynyl]-10,20-diphenylporphinato]metal complexes in which macrocycle conjugation is expanded via ethyne moieties that link the porphyrin 5- and 15- positions to new aromatic entities.[21,66,71] In **7**−**9**, electronic delocalization is evident in the HOMO-3 and the LUMO+3; the former orbital exhibits cumulenic character, while the latter possesses a bridge-localized electron density distribution reminiscent of the HOMO save for the fact that $C_{meso}-C_\alpha$ bonding interactions involving the 5- and 5′-carbon atoms are now absent. The HOMO-1, HOMO-2, LUMO+1, and LUMO+2 manifest substantial porphyrin π-centered electron density (Figure 4A−C) and exhibit no charge localization on the ethynyl bridge. In **7**−**9**, the HOMO-1 and HOMO-2 are a_{1u}/b_2 derived, while the LUMO+1 and LUMO+2 display electron density distributions that derive from linear combinations of the empty $[e_g/(c_1, c_2)]$ frontier orbitals of the monomeric PZn- and PH_2-based building blocks. In **8**, the PZn-localized LUMO+2 lies higher in energy than the corresponding PH_2-localized LUMO+1, as expected, given the relative energies of the corresponding FO's of PH_2 and PZn monomers (Table 4).

Frontier orbital energies were also calculated for pyridine adducts of **7** and **8** (Supporting Information), since electronic absorption and photophysical experiments were performed in 10:1 toluene−pyridine. The calculations show that the minimum energy structures for these species exhibit ruffled PZn units, which serve to destabilize the FOs of **7**-$(pyridine)_2$ and **8**-pyridine relative to those determined respectively for **7** and **8**. It is important to note that the distribution of electron density in the frontier orbitals of **7**-$(pyridine)_2$ and **8**-pyridine does not differ significantly from that displayed pictorially for **7** and **8** in Figure 4.

To probe how small perturbations from idealized symmetry might impact ground- and excited-state electron density distributions in **7**, **8**, and **9**, we performed electronic structure calculations on a THF adduct of a *meso*-to-*meso* ethyne-bridged bis(porphinato)zinc(II) complex analogous to **7 (7′)**,[65] in which the nuclear coordinates were imported from an X-ray crystallographic data file. In the **7′** X-ray crystal structure, the torsional angle between the respective macrocycle least-squares planes is 11.2°.[65] Interestingly, the PZn units of **7′** are structurally inequivalent, exhibiting both different degrees of macrocycle ruffling and conjugation with their respective pendant *meso*-aryl groups. Because **7′** exhibits less than maximal porphyrin−porphyrin conjugation as well as nonplanar macrocycles, its frontier orbitals are destabilized with respect to those elucidated for **7** (Figure 4D, Table 4). Similar to the frontier orbital electron density distributions determined for **8**, asymmetric charge localization is manifest in the HOMO-1, HOMO-2, LUMO+1, and LUMO+2. Whether or not the structural asymmetry evinced in the X-ray crystallographic structure of bis[(5,5′,-10,20-di(*p*-neopentyl benzoate)porphinato)zinc(II)]ethyne results from crystal packing forces or from nuclear displacements that serve to minimize steric interactions involving β-hydrogen atoms that flank the ethyne bridge in the [bis(porphinato)zinc(II)] system,[65] the electronic structure calculations performed on the **7′** structure suggest that dynamical processes that lower the symmetry of species such as **7** may play an important role in determining the condensed-phase optoelectronic properties of *meso*-to-*meso* ethyne-bridged bis(porphyrin) compounds.

(IV) Electroabsorption (Stark) Spectroscopy. Compounds that possess highly polarized electronically excited states often manifest a change in dipole moment ($\Delta\mu_{ge}$) relative to that determined for the ground state. Our ZINDO-based electronic structural studies (Figure 4D) suggest that the highly polarized singlet excited states of **7** and **9** evinced in the transient pump−probe fluorescence anisotropy experiments may possess measurable dipolar character. Because **7** and **9** are electronically symmetric structures, either PZn- or PH_2-localized nuclear distortions that reduce symmetry, or inner solvation shell anisotropy between the left and right halves of these dimers, would be required for the S_1 and S_2 states of these species to exhibit asymmetric distributions of electron density. To probe directly whether dipole moment changes are manifest in the major electronic transitions that make up the B- and Q-absorption envelopes of *meso*-to-*meso* ethyne-bridged bis(porphyrin) complexes fabricated from structurally identical (porphinato)metal or porphyrin macrocycle components, low-temperature electric field effect (Stark) spectroscopy was carried out on compound **7**.

The electroabsorption spectrum of **7** recorded at 77 K is complicated by the presence of multiple unresolved bands (Figure 5). To assess the results quantitatively, the absorption spectrum would have to be deconvoluted into the individual bands comprising the entire spectrum. Since such a deconvolution is dependent on the model employed, coupled with the fact that **7**'s electronic absorption profile evinces significant spectral heterogeneity that derives from a distribution of conformers in solution that differ with respect to the torsional angle between the least-squares planes of its two PZn units,[32,65] such a mathematical fit of the electroabsorption spectra would not necessarily be unique, and thus may lead to artifacts in the assigned electroabsorption parameters. To avoid such ambiguity,

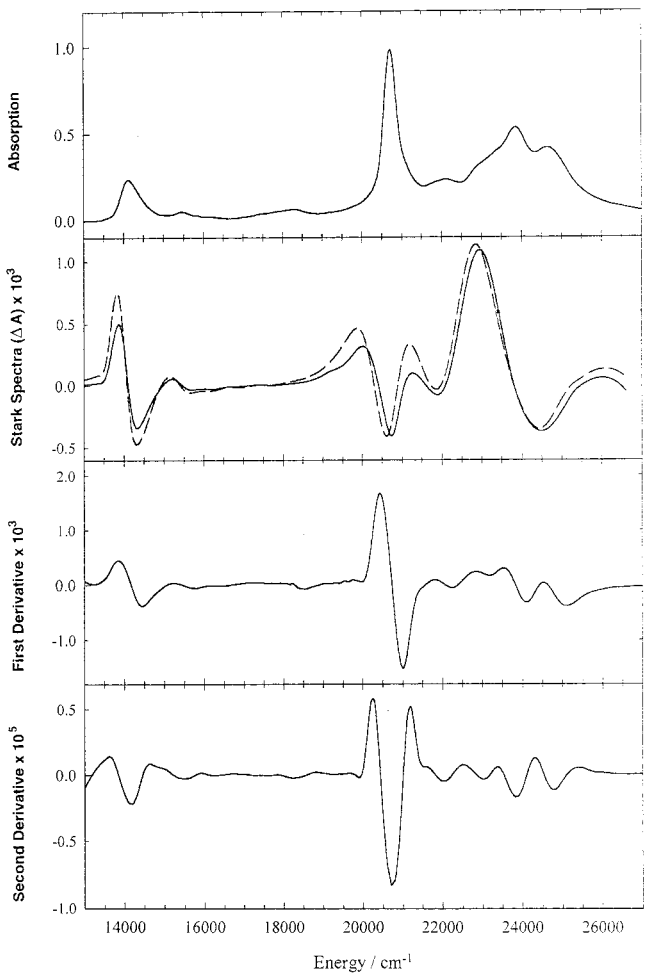

Figure 5. Electronic absorption and electroabsorption data for bis-[(5,5′,-10,20-bis[3″,5″-(di-*tert*-butyl)phenyl]porphinato)zinc(II)]-ethyne (**7**). (A) Absorption spectrum acquired at 77 K in MTHF. (B) Electroabsorption response at $\chi = 90°$ (solid line) and 55° (dashed line). (C) First derivative of the absorption spectrum. (D) Second derivative of the absorption spectrum.

we shall discuss the results in a largely qualitative fashion, pointing out the unique information the Stark experiment provides.

Beginning first with the mid energy region of Figure 5 (19 000 to 22 000 cm^{-1}), it is apparent that the lowest energy transition in the B-band region is reasonably resolved in the Stark spectrum. When compared to the absorption spectrum, it is evident that the line shape contains contributions from both the first and second derivatives, indicating that in addition to the measurable $\Delta\alpha$ present, there is also a contribution due to a change in dipole moment, $\Delta\mu$. Likewise, the Q-state region of the spectrum (Figure 5A) (13 000 to 19 000 cm^{-1}) is quite well resolved at 77 K. While comparison of the Stark spectrum (panel B) to the derivatives of the absorption spectrum (panels C and D) over this energy domain shows that the effect is appreciably first derivative in nature (indicating that the activity can be attributed largely to a change in polarizability), it can be seen as well that there is a second-derivative contribution to the overall line shape of the low-energy Q-state transition centered near 14 000 cm^{-1}. Analyzing these regions of the Stark spectrum, and correcting for local field effects, shows the following: (i) The B-state spectral domain spanning 19 000−22 000 cm^{-1} is characterized by $|\Delta\mu_{ge}|$ and $Tr(\Delta\alpha_{ge})$ values of ~2 D and −6 $Å^3$, respectively, with an estimated *z* component to the latter quantity ($Tr(\Delta\alpha_{ge})$) of −30 $Å^3$. While it is clear that a change in dipole moment occurs with optical excitation of the low-energy B-state, it should be emphasized that the numerical values for $Tr(\Delta\alpha_{ge})$ are less certain because polarizability changes (first derivative contributions) constitute a minor determinant of the Stark spectral line shape. (ii) The low-energy Q-state Stark spectral region is characterized by a large value of $Tr(\Delta\alpha_{ge})$ ($=Tr(\Delta_{az})$) = 460 $Å^3$, which signals a substantial degree of involvement of higher energy empty orbitals in the configuration interaction that describes this S_1 state.[75,76] Consistent with expectations based on conventional descriptions of porphyrin electronic structure, vibronic coupling theory, and simple explanations of observed oscillator strength enhancement of the Q-states through intensity borrowing from the B-states, the second derivative component of the Stark data for the low-energy *x*-polarized Q-state shows that $\Delta\mu_{ge}$ for this transition is also ~2 D. In sum, the data displayed in Figure 5 thus indicate that even for electronically symmetric *meso*-to-*meso* ethyne-bridged bis(porphyrin) complexes, changes in dipole moment that occur in the low-energy *x*-polarized S_2- and S_1-excited states with respect to the ground state likely play a role in maintaining maximal excited-state anisotropy over time scales long with respect to the fluorescence lifetime in compounds **7**−**9**.

While these conclusions are consistent with both electronic structure calculations (vide supra, Figure 4D) and earlier analyses of the optical spectra of related ethyne- and butadiyne-bridged bis- and tris[(porphinato)zinc(II) complexes that feature this linkage topology,[1,2] it is interesting to note that these Stark data differ from that obtained for dimeric and oligomeric butadiyne-bridged (octaalkylporphinato)zinc(II) species examined by Anderson,[23] which show electroabsorption responses that derive exclusively from changes in polarizability. Such spectroscopic differences that exist between these two classes of *meso*-to-*meso* bridged conjugated bis(porphyrins) likely derive from (i) disparate compositions of the S_1 and S_2 excited-state wave functions (in terms of the nature of the configuration expansion) in the Anderson compounds[23,26] relative to those for **7**, which have their genesis from FO electronic perturbations caused by the presence of eight β-alkyl substituents per macrocycle unit in these species, (ii) a differing distribution of ground-state structural conformers in these butadiyne-bridged (octaalkylporphinato)zinc(II) arrays relative to that elucidated for **7**, which features a predominant structural conformer at ambient temperature that has been shown to correspond to a maximally conjugated (approximately planar) geometry,[32,65] or (iii) a combination of these factors.

The highest energy region (22 000 to 27 000 cm^{-1}) is the hardest to interpret, where the presence of multiple bands has yielded a ΔA line shape unlike either the first or second derivatives. There are three obvious possibilities as to why the high-energy region of the Stark spectrum for *meso*-to-*meso* ethyne-bridged bis(porphinato)zinc(II) compounds does not fit well to either a first or second derivative line shape: (i) there is a large zeroth derivative component, indicating that the activity is due to the transition moment polarizability and/or hyperpolarizability, a hypothesis not inconsistent with the demonstrated optoelectronic properties of closely related compounds,[20−22] (ii) in this region of highly overlapping peaks, the Liptay treatment is simply not valid,[59] or (iii) first-derivative behavior dominates, but the extent of the polarizability change is different for different transitions. Based in part on various

(75) Lao, K.; Moore, L. J.; Zhou, H.; Boxer, S. G. *J. Phys. Chem.* **1995**, *99*, 496−500.
(76) Shin, Y.-G. K.; Brunschwig, B. S.; Creutz, C.; Sutin, N. *J. Phys. Chem.* **1996**, *100*, 8157−8169.

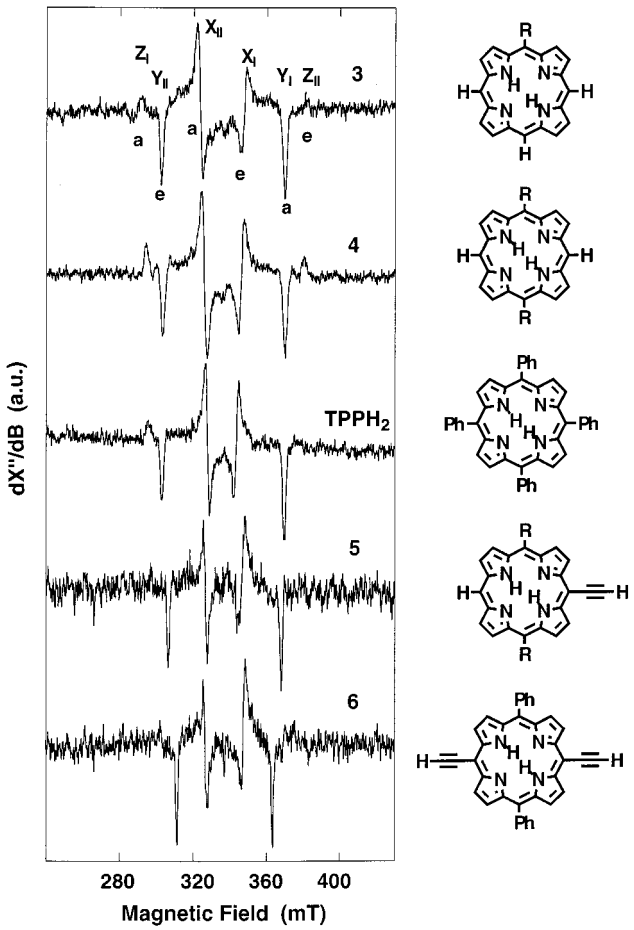

Figure 6. X-band EPR spectra of the photoexcited triplet states of monomeric porphyrins **3**, **4**, **5**, and **6**, as well as in the tetraphenylporphyrin ($TPPH_2$) benchmark. All chromophore concentrations are approximately 1 mM in 10:1 toluene−pyridine (v/v) glassy matrices. Experimental conditions: temperature = 4 K; modulation amplitude = 2.0 mT at 100 kHz; microwave power = 2 μW.

spectral deconvolutions and multiparameter electroabsorbance fits (data not shown), this latter explanation likely accounts for a significant degree of the Stark spectral response in this energy region, and would be consistent with the most prominent Stark features of this B-band spectral domain being indicative of comparatively large $Tr(\Delta\alpha_{ge})$ values (100−300 Å^3). One additional observation can be noted: the relative angular independence observed clearly indicates the Stark signal is not due to a $\Delta\alpha$ or $\Delta\mu$ contribution from a single band. To further delineate the origins of the Stark signal with any greater confidence, however, a better resolved spectrum would be required, such as that which may be obtained at lower temperatures; likewise, higher order Stark measurements might prove to be informative in such an analysis.[75]

(V) Excited Triplet State EPR Spectroscopy. To gain insight into how macrocycle electronic structure affects the distribution of excitation energy within the triplet manifold of *meso*-to-*meso* ethyne-bridged porphyrin arrays, the lowest photoexcited triplet states of unoriented samples of compounds **3**−**9** were studied by electron paramagnetic resonance (EPR) spectroscopy in glassy solvent systems at low temperature (4−100 K) under continuous light irradiation. The results are shown in Figures 6 and 7. The shape of the EPR spectrum of randomly oriented molecules in their excited triplet state depends on the zero-field splitting (ZFS) parameters, and on entry, exit, and spin−lattice relaxation rates of the triplet spin sublevels. The spin Hamiltonian of a triplet spin system is governed mainly

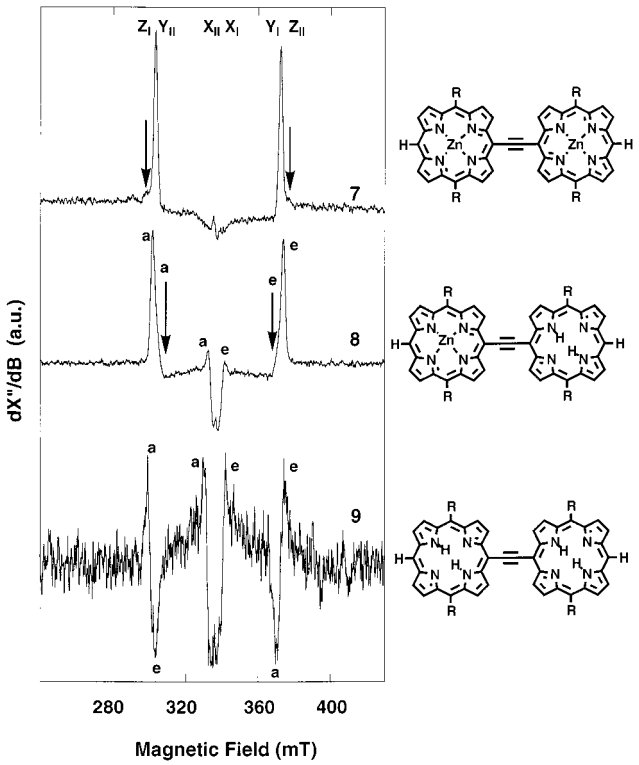

Figure 7. X-band EPR spectra of the photoexcited triplet states of bis(porphyrin) compounds **7**, **8**, and **9**. Arrows denote field positions of Y canonical transitions. All chromophore concentrations are approximately 1 mM in 10:1 toluene−pyridine (v/v) glassy matrices. Experimental conditions: temperature = 4 K; modulation amplitude = 2.0 mT at 100 kHz; microwave power = 2 μW.

by the Zeeman interaction and the dipolar spin−spin interaction of the two electrons in the triplet molecular orbital.[77,78] The nuclear hyperfine couplings are rarely, if at all, seen in randomly oriented triplets in an external field, due to the large degree of anisotropy. Within the molecular axis system, the total spin Hamiltonian describing the Zeeman interaction and the dipolar interaction between the two spins is:

$$H_T = \beta_e \vec{H}\cdot\bar{\bar{g}}\cdot\vec{S} + \vec{S}\cdot\bar{\bar{D}}\cdot\vec{S} \qquad (3)$$

Here $\vec{H}$ is applied magnetic field, β_e the electron Bohr magneton, $\vec{S}$ the total spin, $\bar{\bar{g}}$ the *g*-value tensor, and $\bar{\bar{D}}$ the zero-field splitting tensor which contains contributions from the spin−spin dipolar and spin−orbit interactions. Since the ZFS tensor is traceless, the spin−spin interaction can be recast using two independent parameters, *D* and *E*, giving rise to the familiar phenomenological spin Hamiltonian:

$$H_T + g_e\beta_e\vec{H}\cdot\vec{S} + D\left(S_z^2 - \frac{1}{3}S^2\right) + E(S_x^2 - S_y^2) \qquad (4)$$

The magnitude of the ZFS parameter, $|D|$, is a measure of the electronic spatial distribution of the triplet molecular orbital and is proportional to $\langle r^3\rangle^{-1}$, where *r* is the interelectron distance, while the $|E|$ ZFS parameter is related to the degree of distortion from tetragonal symmetry.[77−79] The quotient $3|E|/|D|$ lies in the range $0 \le 3|E|/|D| \le 1$; here the two extremes represent axial symmetry ($|E| = 0$) and orthorhombic symmetry ($3|E|/|D| =$

(77) Carrington, A.; McLachlan, A. D. *Introduction to Magnetic Resonance*; Chapman and Hall: New York, 1967; pp 115−131 and 204−220.

(78) Weltner, W. *Magnetic Atoms and Molecules*; Dover Publications: New York, 1983.

1).[80] Using a point-dipole approximation, the interelectron distance may be approximated from the $|D|$ value using the following expression,

$$D = \frac{3}{4}\left(\frac{\mu_o}{4\pi}\right)\frac{(g_e\beta_e)^2}{\langle r^3\rangle}\langle 1 - 3\cos^2\theta\rangle \qquad (5)$$

where r is the magnitude of the distance between spin centers, θ is the polar angle describing the relative orientations of the magnetic dipoles, μ_0 is the permeability of free space, and g_e is the free electron g value.

The E ZFS parameter permits assessment of the in-plane spin anisotropy and is given by the following expression:

$$E = \frac{3}{4}\left(\frac{\mu_o}{4\pi}\right)(g_e\beta_e)^2\left\langle\frac{(y^2 - x^2)}{\pi^5}\right\rangle$$

For molecules with a high degree of symmetry (3-fold rotation axis or higher), the term $\langle y^2 - x^2\rangle$ vanishes yielding an E value of zero.

The EPR line shape for randomly oriented triplets has been previously described.[81] The anisotropy of the zero-field splittings, in general, leads to six observable lines or turning points in the first derivative spectrum. Assuming that D is positive, as is commonly observed for planar aromatics, and $E < 0$ (an arbitrary assignment), the $|0\rangle \leftrightarrow |+1\rangle$ transition has Z, X, and Y components at field positions displaced from that of free electron ($h\nu/g_e\beta_e$) by $-D$, $+(D - 3E)/2$, and $+(D + 3E)/2$, corresponding to Z_I, X_I, and Y_I field positions, respectively. Likewise, the $|0\rangle \leftrightarrow |-1\rangle$ transition has lines at field positions displaced from g_e by $+D$, $-(D - 3E)/2$, and $-(D + 3E)/2$ that are defined as the Z_{II}, X_{II}, and Y_{II} transitions, respectively, following the convention of Thurnauer.[82] Thus, from the resulting randomly oriented spectrum, ZFS parameters are readily extractable, with the separations in field units between pairs of transitions given as follows: $\Delta H_z = 2|D|$, $\Delta H_y = |D| + 3|E|$, and $\Delta H_x = |D| - 3|E|$.

Spin state dynamics can be inferred from the EPR excited triplet spectrum under steady-state illumination conditions.[83] Entry into the lowest triplet state is governed primarily by spin−orbit coupling. Consequently, at temperatures (typically in the vicinity of liquid helium) where the $S_0 \leftarrow T_1$ lifetime is short compared to the spin−lattice relaxation time between two spin state sublevels (T_1), a non-Boltzmann occupation (electron spin polarization or, more appropriately, electron spin alignment) of the triplet manifold results. Hence, some transitions will be emissive (**e**) in nature while those that are absorptive (**a**) will be enhanced. The resulting polarization pattern of absorptions and emissions under conditions of steady-state illumination can thus be used to ascertain information concerning intersystem crossing (ISC), spin dynamics, and relaxation.[31,84]

Monomeric Porphyrin Compounds. Photoexcited triplet state EPR spectra for a series of benchmark porphyrin macrocycles are shown in Figure 6; a similar set of spectra for the (porphinato)zinc(II) analogues of these species has been reported previously.[31] As can be seen, all the spectra demonstrate electron spin polarization at 4 K. The **aea-eae** polarization pattern evident for compounds **3**−**6** is consistent with results obtained previously for conventional porphyrin macrocycles under continuous light irradiation.[85,86]

Table 5. Observed Zero-Field Splitting Parameters for Compounds **3**−**9**, PH_2, and $TPPH_2$

compd	solvent[a]	T (K)	$\|D\|$ (cm^{-1})[b]	$\|D\|$ (GHz)[b]	$\|E\|$ (cm^{-1})[b]	$\|E\|$ (GHz)[b]	$3\|E\|/\|D\|$
PH_2	2MTHF	4	0.0436	1.307	0.0065	0.195	0.45
3	tol/pyr	4	0.0412	1.235	0.0058	0.174	0.41
4	tol/pyr	4	0.0409	1.223	0.0074	0.222	0.55
$TPPH_2$	tol/pyr	4	0.0387	1.16	0.0081	0.243	0.63
5	tol/pyr	4	0.0384	1.151	0.0065	0.195	0.51
6	tol/pyr	4	0.0342	1.025	0.0049	0.147	0.43
7	tol/pyr	4	0.0319	0.956	0.0106	0.319	1
8	tol/pyr	4	0.0341	1.022	0.0097	0.291	0.85
9	tol/pyr	4	0.0353	1.058	0.0091	0.273	0.77

[a] tol/pyr = 10:1 pyridine−toluene; 2MTHF = 2-methyltetrahydrofuran (neat). [b] ZFS values ±0.0002 cm^{-1} (0.006 GHz).

The ZFS parameters determined from the photoexcited triplet EPR spectral data for monomeric porphyrin species **3**−**6** are given in Table 5. Several trends emerge from these data. Relative to porphine, the unsubstituted porphyrin macrocycle, the $|D|$ value decreases monotonically with addition of phenyl groups to the *meso* positions of the porphyrin core. For example, the data show that the magnitude of $|D|$ for 5,10,15,20-tetraphenylporphyrin ($TPPH_2$) is diminished by 11% ($|D| = 0.0387$ cm^{-1}) relative to that determined for porphine ($|D| = 0.0436$ cm^{-1}). Similarly, the $|D|$ value decreases with the addition of ethynyl groups to the *meso* position; note that the $|D|$ value of 5,15-diethynyl elaborated compound **6** ($|D| = 0.0342$ cm^{-1}) is reduced 22% relative to porphine ($|D| = 0.0436$ cm^{-1}) and 16% relative to 5,15-diphenylporphyrin (compound **4**) ($|D| = 0.0409$ cm^{-1}). Using the simple point-dipole approximation and eq 5, the calculated interelectron distance in the photoexcited triplet state of porphine is 3.10 Å, 0.14 Å less than that manifest in $TPPH_2$. For the *meso*-ethyne-elaborated porphyrins **5** and **6**, the respective interelectron distances are estimated to be 3.24 and 3.36 Å, indicating that the spatial extent of the triplet wave function is greater in these compounds. Of particular note is the reduction in line width of the stationary field transitions in the ethyne-elaborated porphyrins relative to $TPPH_2$, **3**, and **4**; the line widths of the low-field Y-transition of these species lie in the range 2.0−2.2 mT, whereas for ethyne-elaborated **5** and **6**, the relevant line widths are respectively 1.6 and 1.3 mT. These data are consistent with both the expansion of the triplet-state electron spin density out onto the ethynyl moieties of species **5** and **6** and the concomitant reduction of the magnitude of nitrogen-localized spin density in the T_1 states of these compounds with respect to that typically observed in the analogous excited states of less conjugated porphyrin macrocycles (**3**, **4**, and $TPPH_2$).

***Meso*-to-*Meso* Ethyne-Bridged Bis(porphyrin) Species.** The photoexcited triplet state EPR spectra of compounds **7**−**9** in the $|\Delta M_s| = 1$ region are shown in Figure 7; the ZFS parameters are given in Table 5. The spectrum obtained for **7** is virtually identical with that reported previously for bis[(5,5′,-(10,20-diphenylporphinato)zinc(II)]ethyne.[31] Interestingly, the low-temperature photoexcited triplet EPR spectrum of **8** bears a striking similarity to that obtained for **7** (Figure 7), suggesting that the electronic structures of their respective T_1 states are related. The polarization patterns of **7** and **8** are **aaa-eee**,

(79) Weil, J. A.; Bolton, J. R.; Wertz, J. E. *Electron Paramagnetic Resonance*; J. Wiley and Sons: New York, 1994,
(80) Poole, C. P.; Farach, H. A. *J. Chem. Phys.* **1974**, *61*, 2220−2221.
(81) Kottis, P.; Lefebvre, R. *J. Chem. Phys.* **1963**, *39*, 393−403.
(82) Thurnauer, M. C. *Rev. Chem. Intermed.* **1979**, *3*, 197−230.
(83) Thurnauer, M. C.; Katz, J. J.; Norris, J. R. *Proc. Natl. Acad. Sci. U.S.A.* **1975**, *72*, 3270−3274.
(84) *Optical Spin Polarization in Molecular Crystals*; Waugh, J. S., Ed.; Academic Press: New York, 1976; Vol. 8, pp 85−121.
(85) Kleibeuker, J. F.; Schaafsma, T. J. *Chem. Phys. Lett.* **1974**, *29*, 116−122.
(86) Ponte Goncalves, A. M.; Burgner, R. P. *J. Chem. Phys.* **1976**, *65*, 1221−1222.

signaling that entry into the triplet manifold is governed by spin−orbit coupling and directed into the $|T_z\rangle$ spin sublevel. The $|D|$ value evaluated for compound **8** ($|D| = 0.0341$ cm^{-1}) is larger than that determined for **7** ($|D| = 0.0319$ cm^{-1}), indicating that spin delocalization in **7** is marginally greater. The EPR spectrum of the photoexcited triplet state of **9** (Figure 7) possesses a polarization pattern of **aea-eae** typical of that evinced for monomeric free-base porphyrin macrocycles (Figure 6). The $|D|$ value for **9**, however, is augmented relative to that observed for both **7** and **8** (Table 5); note that the calculated T_1-state interelectron distance for **9** (3.30 Å) is similar to that estimated for 5,15-diethynyl-10,20-diphenylporphyrin (**6**).

Variable-temperature EPR spectroscopic studies (4−100 K) of the photoexcited triplet state of compound **8** reveal that the line shape of the triplet EPR spectrum maintains the hallmarks of rhombic symmetry ($|D| \geq 3|E|$), neither changing its polarization profile nor developing stationary field transitions with an $|E|$ value ≈ 0 as the temperature is increased (Supporting Information); thus, there is no evidence up to 100 K for the dynamic Jahn−Teller effect, as seen in many metalloporphyrin triplet state systems which exhibit more pronounced axial triplet components with increasing temperature.[31,87−89] Moreover, as with compound **7**, this species is unusual in that there is little evidence of thermalization between spin sublevels up to 100 K. This points to the fact that the magnitudes of entry, exit, and inter-spin sublevel transition rate constants are such that spin polarization is maintained over a wide temperature range,[31] consistent with previously reported data for electronically symmetric bis[(5,5′-10,20-diphenylporphinato)zinc(II)]ethyne (**7″**).

One important issue in these systems regards the spatial extent of both the excited singlet and lowest triplet excitations. It has been previously demonstrated for closed-shell PZn-based multichromophore arrays in which ethyne or butadiyne units bridge the constituent macrocycles at their respective *meso*-carbon positions, that the triplet state electronic structure is perturbed with respect to that observed for analogous β-to-β and *meso*-to-β linked multiporphyrin compounds.[31] The photoexcited triplet states of *meso*-to-*meso* ethyne- and butadiyne-bridged PZn arrays manifest a reorientation of the axis of greatest dipolar coupling from *Z* (perpendicular to the porphyrin plane) to *X* (along the highly conjugated *meso*-to-*meso* bridge); this reorientation occurs concomitant with a decrease in the $|D|$ ZFS parameter. This oblate-to-prolate spin transition observed for **7″** (and its bis[(porphinato)zinc(II)] analogue that featured a *meso*-to-*meso* butadiyne linker) in the lowest photoexcited triplet state correlated with the enhanced chromophore−chromophore coupling made possible by this linkage topology relative to that determined for corresponding bis(chromophoric) complexes that possessed *meso*-to-β or β-to-β bridging motifs.[1,2,31] Similar reorientations of the axis of largest dipolar coupling have been observed in the photoexcited triplet EPR spectra of stretched porphycenes and the sapphyrin dication.[90,91]

As emphasized above, in the limit of $3|E|/|D| = 1$, the spin distribution assumes orthorhombic symmetry; in such a case the *Z* and *Y* canonical transitions overlap and the corresponding low- and high-field *X* transitions become equivalent at approximately $g = 2.00$ (320 mT). As observed for PZn species at low temperature,[31] the X transitions carry spin polarization such that the low-field transition is enhanced in absorption while the high-field transition is enhanced in emission. When these spin-polarized transitions overlap in the orthorhombic limit, they result in essentially zero signal in the photoexcited EPR spectrum. As exemplified in compound **8** (Figure 7), the *Y* canonical transitions are nearly overlapping the *Z* transitions (arrows, Figure 7), resulting in a ratio of $3|E|/|D| = 0.85$. In **7**, it is clearly evident that the X_I and X_{II} transitions are overlapping at $g = 2.00$; because the former transition is absorptive and the latter is emissive, the signal displays almost no net intensity. Furthermore, it is apparent as well that the *Y* transitions are crossing over what were the *Z* transitions (arrows, Figure 7). The axis of largest dipolar coupling is along the standard *Z* (perpendicular to the porphyrin plane) direction in **8**'s low-energy photoexcited triplet state; this clearly differs in compound **7**, in which a redistribution of spin density in the photoexcited triplet state is observed to occur, causing the axis of largest dipolar coupling to align along *Y* (an axis lying in-plane and along the axis of conjugation). Using the point-dipole approximation (eq 5), **7**'s T_1-state interelectron separation can be estimated to be 4.3 Å, approximately 1 Å larger that that calculated for the monomeric PZn and PH_2 compounds (PH_2, $TPPH_2$, and **3**−**6**) examined in this study. While the T_1-state interelectron distance undoubtedly increases concomitant with the oblate-to-prolate spin redistribution, given the head-to-tail orientation of the dipolar interaction and the potentially complex nature of the T_1 wave function, this calculated interelectron separation should only be viewed as a very rough approximation.

A similar evolution toward the orthorhombic limit is also observed in **9**'s photoexcited triplet state EPR spectrum, which clearly differs from the spectra elucidated for monomeric compounds (**3**−**6**) (Figure 6). As is evident from Table 5, the simple porphyrin macrocycles have ($3|E|/|D|$) ratios in the range 0.41−0.63, whereas the value for **9** is 0.77. The *E* ZFS parameter decreases (becomes more axial) with increasing conjugation in mono- and di-*meso*-ethyne elaborated compounds **5** (0.0065 cm^{-1}) and **6** (0.0049 cm^{-1}) relative to the parent diphenylporphyrin macrocycle **4** (0.0074 cm^{-1}). This evolution in the $|E|$ ZFS parameter with augmented conjugation is consistent with a progressing rotation of the porphyrin principal axis system that causes the direction of largest dipolar interaction to evolve along the vector defined by the conjugated ethyne moiety. Changes in the magnetic anisotropy of the photoexcited triplet states of compounds **4**−**9** are thus seen to mirror the changes evinced in the excited-state polarization of the S_1 states of these species demonstrated in the fluorescence anisotropy measurements, signaling that the magnetic and optical principal axis systems migrate with increasing conjugation toward an identical reference frame.

Although the triplet lifetimes of the dimeric arrays **7**−**9** are shorter by about an order of magnitude (vide infra) relative to benchmark monomeric PH_2 and PZn compounds, continuous illumination still provides significant steady state population within the triplet manifold. As noted above, the magnitudes of the evaluated $|D|$ parameters are significantly greater than those expected for globally delocalized triplet excitation in compounds **7**−**9**; moreover, the fact that the photoexcited triplet EPR spectrum of electronically asymmetric **8** evinces only excitation localization on the PZn moiety and shows no absorptive and emissive signatures characteristic of a PH_2 triplet further underscores this point. While the origin for the observed

(87) Angiolillo, P. J.; Vanderkooi, J. M. *Biophys. J.* **1995**, *68*, 2505−2518.
(88) Angiolillo, P. J.; Vanderkooi, J. M. *Biophys. J.* **1998**, *75*, 1491−1502.
(89) *Electron Spin Resonance of Porphyrin Excited States*; Dolphin, D., Ed.; Academic Press: New York, 1979; Vol. IV, pp 257−312.
(90) Levanon, H.; Regev, A.; Michaeli, S.; Galili, T.; Cyr, M.; Sessler, J. *Chem. Phys. Lett.* **1990**, *174*, 235−240.
(91) Berman, A.; Levanon, H.; Vogel, E.; Jux, N. *Chem. Phys. Lett.* **1993**, *211*, 549−554.

localization of triplet excitation on **8**'s PZn unit is not entirely clear, appending ethyne moieties to the (porphinato)zinc(II) macrocycle clearly breaks the degeneracy in the lowest photoexcited triplet state (^3E_u in D_{4h} point group). Due to the lack of any temperature-dependent dynamic Jahn−Teller effects of the EPR line shape up to temperatures of approximately 100 K, the energy separation between these two vibronically split triplet states must be greater than 150 cm^{-1} ($2k_BT$ at 100 K).[31] The magnitude of the rectangular distortion that occurs in the photoexcited triplet state of a (5-ethynylporphinato)zinc(II) moiety must exceed that in the analogous 5-ethynylporphyrin species to account for the unusual finding that the lowest energy triplet state of a PZn−PH_2 compound is PZn localized.[34,36] While intramolecular spin polarization transfer from the PZn to PH_2 units cannot be unequivocally ruled out in compound **8**'s electronically excited low-temperature triplet state, it is important to note that in systems where such triplet spin polarization transfer is known to occur, the $|D|$ ZFS parameter that is observed in the triplet EPR spectrum is that of the acceptor molecule (for an intermolecular energy transfer) or the acceptor moiety of a D−Sp−A assembly.[92,93] Furthermore, in compound **8**, the $|D|$ ZFS parameter is 0.0341 cm^{-1}, significantly lower than any of the monomeric porphyrin macrocycles studied (Table 5), consistent with the notion as well that intramolecular spin polarization transfer is not the genesis of the features manifest in compound **8**'s low-temperature triplet EPR spectrum.

Localization of triplet excitation is commonly manifest in oligomeric, π-conjugated, arene, and heterocycle systems;[94−98] in oligothiophenes, for example, optically detected magnetic resonance studies of the lowest energy triplet state indicate that the spatial extent of the excitation does not span more than one thiophene ring.[95] More recent studies using pulsed EPR methods have similarly shown that oligothiophenes that feature two through eight heterocyclic units demonstrate analogous excitation confinement in the lowest photoexcited triplet state.[94] Likewise, the time-resolved EPR spectroscopy of the photoexcited triplet states of several phenylene-linked (porphinato)metal and porphyrin-based bis(chromophore)species shows that on the time scale probed by field swept EPR, the triplet excitation appears to be localized on a single porphyrinic unit;[99] it must be emphasized, however, that this technique does not rule out the possibility of slow to intermediate exchange with correlation times $\leq 10^{-8}$ s.

One obvious point to consider is whether the observed triplet EPR signals in species **7**−**9** derive from the bulk sample, or from a subset of conformational isomers in the frozen matrix in which the dihedral angle between the respective porphyrin macrocycles in these conjugated bis(pigment) complexes spans a narrow range. For example, it could be hypothesized that the photoexcited triplet states of **7**−**9** probed in these experiments derive exclusively from a conformeric subpopulation in which the two macrocycles of the conjugated bis(chromophoric) system feature an approximately orthogonal mutual orientation. Using a binucleating 4,4′-dipyridyl axial ligand, compound **7**, and experimental conditions that generate significant concentrations of face-to-face dimeric structures that ensure a mutually coplanar arrangement of the ethyne-bridged[(porphinato)zinc(II)] units,[100] photoexcited triplet EPR spectra were obtained that were indistinguishable from that displayed for **7** in Figure 7. Furthermore, the intensities of the observed spectral signals as a function of time in these experiments are approximately identical for a given concentration **7**, whether or not the binucleating ligand is present (data not shown). These data suggest that the apparent extent of triplet state wave function localization in **7**−**9** is not particularly sensitive to the magnitude of the dihedral angle manifest between the planes of the component porphyrin macrocycles.

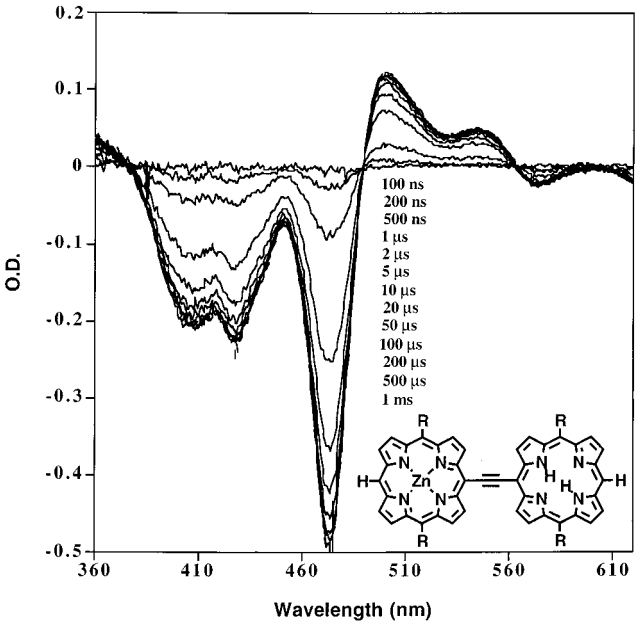

Figure 8. Transient triplet−triplet absorption spectra of compound **8**. Experimental conditions: temperature = 25 °C; λ_{ex} = 700 nm; solvent = 10:1 toluene−pyridine; concentration = 2×10^{-6} M.

Congruent with CW-EPR spectroscopic studies of the lowest photoexcited triplet states of an extensive family of highly conjugated PZn arrays, this study strongly suggests that in the low-temperature regime (4−100 K) over the time scale probed by the ZFS ($\sim 10^{-9}$ s), triplet excitation is confined in compounds **7**−**9**, with interelectron separations not exceeding dimensions in excess of a single porphyrinic unit and its pendant ethynyl moieties.[31] The T_1 states of these systems thus bear resemblance to the low-energy triplet states of oligophenylene ethynylene species, in which unusually large lattice relaxations drive localization of the T_1 exciton, restricting the spatial extent of this wave function with respect to that for S_1, S_n, and T_n excited states.[94−98]

(VI) Transient Triplet−Triplet Absorption Spectroscopy. Transient triplet−triplet ($T_1 \rightarrow T_n$) absorption measurements of a series of ethyne- and butadiyne-bridged PZn arrays indicated that the lowest triplet excited state localizes on a single porphyrin chromophore.[31] Similar studies were performed on **7**, **8**, and **9** in 10:1 toluene−pyridine at room temperature. A triplet−triplet absorption spectrum for compound **8** is shown in Figure 8; triplet−triplet absorption spectra for compounds **7** and **9** are available as Supporting Information. The observed reduction in T_1-state absorption intensity from **7** → **8** → **9** is consistent with the fact that the extent of spin−orbit coupling in PH_2

(92) Akiyama, K.; Tero-Kubota, S. *Mol. Phys.* **1994**, *83*, 1091−1097.
(93) Imamura, T.; Onitsuka, O.; Murai, H.; Obi, K. *J. Phys. Chem.* **1984**, *88*, 4028−4031.
(94) Bennati, M.; Grupp, A.; Mehring, M.; Bauerle, P. *J. Phys. Chem.* **1996**, *100*, 2849−2853.
(95) Swanson, L. S.; Shinar, J.; Yoshino, K. *Phys. Rev. Lett.* **1990**, *65*, 1140−1143.
(96) Beljonne, D.; Cornil, J.; Friend, R. H.; Janssen, R. A. J.; Brédas, J. L. *J. Am. Chem. Soc.* **1996**, *118*, 6453−6461.
(97) Bennati, M.; Nemaeth, K.; Surjan, P. R.; Mehring, M. *J. Chem. Phys.* **1996**, *105*, 4441−4447.
(98) Beljonne, D.; Wittmann, H. F.; Köhler, A.; Graham, S.; Younus, M.; Lewis, J.; Raithby, P. R.; Khan, M. S.; Friend, R. H.; Brédas, J. L. *J. Chem. Phys.* **1996**, *105*, 3868−3877.
(99) Jaegermann, P.; Plato, M.; von Maltzan, B.; Mobius, K. *Mol. Phys.* **1993**, *78*, 1057−1074.

Table 6. Triplet Excited State Lifetime Data of Compounds **7**−**9** Determined from Transient Absorption Experiments[a,b]

compd	absorption decay (μs)	bleach recovery (μs)
7	194 ± 13	190 ± 10
8	130 ± 12	109 ± 11
9	122 ± 9	158 ± 8

[a] Experimental conditions: T = 25 °C, pump wavelength = 700 nm, solvent = 10:1 toluene−pyridine; concentration = 2×10^{-6} M. The time-resolved data could be fit as single exponential decays over a minimum of 5 lifetimes. Analyses of the goodness of the data fit correspond to minimum values of χ^2 of 0.990. Wavelengths chosen for monitoring transient absorption and bleaching were those where ground-state bleaching is minimal. [b] Rate constants reported ± their standard errors.

macrocycles is significantly less than that in their PZn counterparts due to reduced intersystem crossing (ISC) efficiency (Figure 8; Supporting Information). The spectra are characterized by a bleach in the Soret region and absorption at longer wavelengths; consistent with the fact that compounds **8** and **9** exhibit more prominent electronic absorptions in the 500−620 nm spectral domain with respect to complex **7** (Figure 2), additional ground-state bleaching is observed in this region of the triplet−triplet absorption spectra for these compounds relative to that seen in the analogous spectrum for **7**. The $T_1 \rightarrow T_n$ absorbance spectra exhibited by these conjugated bis(porphyrin) compounds are similar to the $T_1 \rightarrow T_n$ absorbance spectrum observed for TPPZn;[101] this suggests that the $T_1 \rightarrow T_n$ transition observed in **7**−**9** generates a $^3(\pi,\pi^*)$ excited state closely related to the doubly excited electronic configuration ($a_{1u}^1\ a_{2u}^1 e_g^1\ e_g^1$). These results are both consistent with photoinduced triplet−triplet absorption experiments carried out with an extensive series of ethyne- and butadiyne-bridged bis- and tris(porphinato)zinc(II) compounds and congruent with the EPR spectroscopic data which show that the triplet excitation is essentially localized on one porphyrin macrocycle in the bis(porphyrin) compounds **7**−**9**.[31] The $T_1 \rightarrow T_n$ absorption band maxima occur at 516, 502, and 494 nm, respectively, for compounds **7**, **8**, and **9**, and lie 2000−3000 cm^{-1} to the red of the analogous $T_1 \rightarrow T_n$ absorption observed for TPPZn (469 nm, toluene−pyridine)[31,101] and $TPPH_2$ (430 nm, toluene).[102] Isosbestic points observed in the triplet−triplet absorption spectra for **7**−**9** (Figure 8, Supporting Information) suggest in each case the formation of a single photoexcited species. The evaluated time constants for ground-state recovery for complexes **7**−**9** derived from the transient triplet−triplet absorption spectra are monoexponential when evaluated at absorption decay and bleach recovery wavelengths where ground-state bleaching is minimal (Table 6). For **7** and **8**, the absorption decays and the bleach recovers with indistinguishable lifetimes (**7**, 194 ± 13 and 190 ± 10 μs; **8**, 130 ± 12 and 109 ± 11 μs); for **9**, the evaluated time constant of the bleach recovery (157 ± 11 μs) is slightly longer than that observed for the absorption decay (122 ± 9 μs). The triplet lifetimes of conjugated bis(porphyrin) compounds **7**−**9** are diminished with respect to that reported for $TPPH_2$ (447 μs) and TPPZn (526 μs) in toluene at 283 K,[102] consistent with a slightly reduced energy gap between the T_1 and S_0 states of **7**−**9** relative to that manifest in these benchmark chromophores. Interestingly, the fact that the lifetime of the T_1 excited state for electronically asymmetric **8** is similar in magnitude to that observed for the conjugated bis(PZn) and bis(PH_2) complexes **7** and **9** suggests that there are no low-lying charge resonance states that serve to efficiently deactivate its photoexcited triplet state.

Conclusions

Expansion of conjugation at the *meso*-carbon positions via ethyne moieties in porphyrin and (porphinato)metal systems effects an electronic structural perturbation that results in enhanced nonbonding character in the porphyrin-localized frontier orbitals relative to the parent PH_2 and PZn compounds that feature conventional *meso*-aryl substituents; this perturbation is exceptionally pronounced in multiporphyrin systems that feature *meso*-to-*meso* ethynyl linkages. The absorption and emission data obtained for *meso*-to-*meso* ethyne-bridged bis(porphyrin) complexes **7**−**9** suggest that the nature of their respective S_1 excited states is similar. These data also reveal that relative to the differences in electronic structure that exist between PH_2 and PZn building blocks, the electronic perturbation to the frontier orbitals that derives from the existence of the *meso*-to-*meso* ethyne bridge is extreme, and constitutes the primary determinant of the nature of the S_1 excited state and the redistribution of electron density that accompanies the S_0−S_1 transition for these conjugated bis(porphyrin) chromophores.

Pump−probe fluorescence anisotropy experiments show that the presence of *meso*-ethynyl substituents drives a reorientation of orthogonal *x*- and *y*-polarized singlet excited states in the macrocycle frame of reference with respect to that evinced for conventional free-base porphyrin chromophores. In mono- and diethyne-elaborated **5** and **6**, for example, it can be seen that the lowest energy S_1-excited state is no longer polarized along the vector that bisects the pair of proton-bearing nitrogen atoms in the macrocycle core; the orientation of the low-energy Q_x state has rotated toward the *meso*-carbon positions that bear the ethyne substituents, redefining the porphyrin principal optical axis system. Analogous experiments carried out with conjugated bis(porphyrin) complexes **7**−**9** show that the large energetic splitting of the *x*- and *y*-polarized S_1 states completely suppresses *x*- and *y*-polarized excited-state population exchange on the time scale (ns) of these measurements, giving rise to singly degenerate emitting states polarized exclusively along the axis defined by the ethyne moiety. In sum, these data underscore the pivotal role of the ethyne moiety in determining the nature of the ground and excited states of these compounds and show quite convincingly that (i) the electronic perturbation induced by conjugation expansion mediated by the ethyne moiety significantly exceeds that which derives from the electronic asymmetry of the pyrrole rings of PH_2 macrocycles (compound **9**) and (ii) moderate differences between the energies and symmetries of the frontier orbitals of the monomeric pigment building blocks of *meso*-to-*meso* ethyne-linked porphyrin arrays neither cause S_1-state excitation localization nor reduce the degree of excited-state polarization.

Data provided by ZINDO-based electronic structure calculations are consistent with the description of the singlet excited states that emerges from the optical spectroscopy and photophysics of the conjugated bis(porphyrin) complexes and their corresponding ethyne-elaborated porphyrin building blocks. Importantly, these studies suggested that dynamical processes that lower the symmetry of complexes such as **7** may play an important role in determining the condensed-phase optoelectronic properties of *meso*-to-*meso* ethyne-bridged bis(porphyrin) compounds. Stark spectroscopic experiments substantiate this hypothesis, demonstrating that even for an electronically sym-

(100) Anderson, H. L. *Inorg. Chem.* **1994**, *33*, 972−981.
(101) Walters, V. A.; de Paula, J. C.; Jackson, B.; Nutaitis, C.; Hall, K.; Lind, J.; Cardozo, K.; Chandran, K.; Raible, D.; Phillips, C. M. *J. Phys. Chem.* **1995**, *99*, 1166−1171.
(102) Fujisawa, J.; Ohba, Y.; Yamauchi, S. *J. Am. Chem. Soc.* **1997**, *119*, 8736−8737.

metric *meso*-to-*meso* ethyne-bridged bis[(porphinato)zinc(II)] complex, changes in dipole moment with respect to the ground state are evinced in the *x*-polarized S_2 and S_1 states; these data highlight the importance of cumulenic character in these excited electronic configurations,[1,2] and strongly suggest that changes in dipole moment with respect to the ground state likely play a role in maintaining maximal excited-state anisotropy over time scales long with respect to the fluorescence lifetime in compounds **7**−**9**.

Spectroscopic studies of the low-lying photoexcited triplet states of these complexes evince a number of unusual properties. The triplet state EPR spectrum of mono- and diethyne-elaborated complexes **5** and **6** manifest electron spin density delocalization onto the ethynyl moieties with concomitant reduction of the magnitude of nitrogen-localized spin density, contrasting the T_1 state spectral features typically observed for less conjugated porphyrin macrocycles (**3**, **4**, and $TPPH_2$). There is no evidence up to 100 K for thermalization between spin sublevels, as is seen in many porphyrin triplet state systems; these data demonstrate that the magnitudes of entry, exit, and inter-spin sublevel transition rate constants are such that spin polarization is maintained over a wide temperature range.

The photoexcited triplet EPR spectrum of electronically asymmetric compound **8** contrasts that of the *meso*-to-*meso* ethyne-bridged bis(porphyrin) complexes (**9**), and exhibits ZFS parameters as well as a line shape and a spin polarization pattern consistent with that of a closed shell metalloporphyrin triplet excited state. These data suggest that the magnitude of the rectangular distortion that occurs in the photoexcited triplet state of a (5-ethynylporphinato)zinc(II) moiety must exceed that in the analogous 5-ethynylporphyrin species and stand in marked contrast to the T_1 states of conventional, covalently linked, PZn−PH_2 systems that do not preserve conjugation between the porphyrin moieties. Interestingly, because transient triplet−triplet transient absorption spectroscopic data show that the lifetime of **8**'s T_1 excited state is similar in magnitude to that observed for bis(PZn) and bis(PH_2) complexes **7** and **9**, one must conclude that there are no low-lying charge resonance states that serve to efficiently deactivate its T_1 state.

The evolution in the $|D|$ and $|E|$ ZFS parameters with augmented conjugation in these species is consistent with a progressing oblate-to-prolate spin transition (a rotation of the porphyrin principal magnetic axis system) that causes the direction of largest dipolar interaction to align along the vector defined by the conjugated ethyne moiety. Changes in the magnetic anisotropy of the photoexcited triplet states of compounds **4**−**9** mirror the changes evinced in the excited-state polarization of the S_1 states of these species demonstrated in the fluorescence anisotropy measurements; the magnetic and optical principal axis systems thus evolve with increasing conjugation toward an *identical* reference frame. Conjugated arrays based on *meso*-ethyne elaborated PZn and PH_2 precursors thus constitute an unusual class of oligomeric porphyrin species in that once a threshold level of conjugation is reached, the optical and magnetic principal axis systems become coincident; such systems may provide interesting platforms in which to optically modulate energy migration events within a photoexcited triplet manifold.

Acknowledgment. M.J.T. is indebted to the NIH (GM 48130-6) and the MRSEC Program of the National Science Foundation (DMR-96-32598) for their research support, and to the Searle Scholars Program (Chicago Community Trust), the Arnold and Mabel Beckman Foundation, E. I. du Pont de Nemours, and the National Science Foundation for Young Investigator Awards, as well as to the Alfred P. Sloan and Camille and Henry Dreyfus Foundations for research fellowships. J.T.H. gratefully acknowledges research support from the United States Department of Energy (DE-FG02-87ER13808). The authors thank Drs. Victor S.-Y. Lin, Laba Karki, Fredrick W. Vance, and Robert J. Stanley for many helpful and stimulating discussions. Transient fluorescence anisotropy measurements were performed at the NIH-supported (RR01348) Regional Laser and Biotechnology Laboratory (RLBL) at the University of Pennsylvania.

Supporting Information Available: Syntheses and characterization data, optical spectra, temperature-dependent X-band photoexcited triplet EPR spectra (compound **8**), transient triplet−triplet absorption spectra (compounds **7** and **9**), along with the frontier molecular orbitals determined for **7**-$(pyridine)_2$, **8**-(pyridine), and a selection of benchmark porphyrin and (porphinato)zinc(II) species (PDF). This material is available free of charge via the Internet at http://pubs.acs.org.

JA9939587